

POLITECNICO DI TORINO



Department of Mechanical and Aerospace Engineering (DIMEAS)

Master of Science in Biomedical Engineering

Fabrication and characterization of nanoparticles-containing melt electrowritten scaffolds for bone cancer treatment

Supervisors

Prof. Enrica Vernè

Prof. Marta Miola

Internship tutor

Prof. Aldo R. Boccaccini

Candidate

Ilenia Occhipinti

279978

a.a. 2021/2022

Abstract

This thesis aims to develop a PCL scaffold with magnetic (M) nanoparticles (NPs) or core-shell magnetic-silica nanoparticles (Si-MNPs) coating for bone cancer applications. Scaffolds were produced with Bioscaffolder 3.1 (Gesim) melt electro-writing (MEW), a high-resolution additive manufacturing (AM) method for printing highly porous scaffolds composed of synthetic biodegradable polymers. In the beginning, PCL (Gesim) from the printer was used, later it was replaced by PCL from Sigma Aldrich (45kDa). Then, after an alkaline treatment on the scaffold surface (for 1h, 2h, and 3h), MNPs and Si-MNPs coatings were synthesized. Afterward, the scaffold's chemical, physical, and biological properties were investigated. In particular, Scanning Electron Microscopy (SEM) images illustrated the morphology of the scaffold's fibers. For Gesim PCL the average fiber size was $44 \pm 1 \mu\text{m}$, while for PCL (45kDa) the average fiber size was $31 \pm 3 \mu\text{m}$. With the alkaline treatment, in both cases, fiber size decreases. SEM images showed also the presence of MNPs and Si-MNPs coating. The chemical structure of the scaffolds and the MNPs and Si-MNPs' presence was determined by Attenuated Total Reflection – Fourier transform infrared spectroscopy (ATR-FTIR). The mechanical test showed that there was no relevant difference in Young's Modulus of PCL, PCL with alkaline treatment, and with MNPs or Si-MNPs scaffolds. Subsequently, the NPs stability in the DMEM medium was analyzed after 1 day and 7 days, by measuring the pH of the medium and by ATR-FTIR of the samples evidencing a probable release of both MNPs and Si-MNPs. The wettability analysis and the antioxidant activity, performed using DPPH assay, displayed successful surface modification after 3 hours of alkaline treatment: the wettability increased, and the color of DPPH solution changed, as proof of alkaline treatment. The antioxidant activity increased from 4% for PCL scaffolds to 16% for scaffolds with MNPs and Si-MNPs coating. The antibacterial study was carried out by direct turbidity assay with *E. coli* and *S. aureus* bacteria for 3h, 6h, and 24h. The results showed that the incorporation of MNPs has a slightly antibacterial effect for *S. aureus* and *E. coli* strains at 6h. Finally, biological activity was studied: cytotoxicity was analyzed using osteoblast-like osteosarcoma MG-63 cells, which showed that the samples were non-toxic. Subsequently, cell proliferation of osteoblastic M3T3-E1 cells was analyzed after 1 day and 7 days and by fluorescence staining, it was observed that the cells proliferated in PCL scaffolds with MNPs and Si-MNPs coating. In conclusion, the results showed that the PCL scaffold with MNPs or Si-MNPs had good physical, mechanical and biological properties and was a potential candidate for bone cancer applications.

INDEX

1 Introduction	1
1.1 Bone cancer	1
1.1.1 Osteosarcoma, Ewing sarcoma, Chondrosarcoma	1
1.1.2 Principal bone cancer treatments	2
1.2 Biomaterials for bone tumor therapy	2
1.3 Nanoparticles	4
1.3.1 Nanomedicine	4
1.3.2 Magnetic Nanoparticles	6
1.3.2.1 Magnetic Properties	6
1.3.2.2 Properties of Magnetic Nanoparticles for biomedical applications	7
1.3.2.3 Synthesis of Magnetic Nanoparticles	8
1.3.2.4 Application of Magnetic Nanoparticles in biomedical field	9
1.3.2.5 Core-shell Magnetic-Silica Nanoparticles	10
1.4 Melt-Electrowriting	11
1.4.1 Melt-Electrowriting Technique	11
1.4.2 Polycaprolactone	12
1.4.3 PCL scaffold with MNPs coating in bone cancer applications	13
Materials & Methods	15
2.1 Materials	15
2.2 Methods	16
2.2.1 Preparation PCL	16
2.2.2 Melt electrowritten scaffold	16
2.2.2.1 MEW scaffold parameters	16
2.2.2.2 Temperature measurement	17
2.2.3 Surface modification with alkaline hydrolysis treatment	17
2.2.4 Magnetic nanoparticles coating	17
2.2.4.1 Magnetic nanoparticles preparation	17
2.2.4.2 Citric Acid dispersion	18
2.2.4.3 Silica shell coating	19
2.2.4.4 PCL melt electrowritten scaffolds with MNPs and Si-MNPs coating	19
2.2.5 Characterization	19
2.2.5.1 Surface morphology	19
2.2.5.2 Surface chemistry	19
2.2.6 Release of MNPs and Si-MNPs in medium	21
2.2.7 Mechanical strength test	21
2.2.8 Antioxidant Activity	21
2.2.9 Antibacterial Activity	22
2.2.10 Biological Activity	23
2.2.10.1 Cell Culture	23
2.2.10.2 Cytotoxicity	23
2.2.10.3 Cell proliferation	24
2.2.10.4 Cell morphology – Fluorescent cell staining	25
3 Results & Discussion	27
3.1 Melt electrowritten scaffolds	27
3.1.1 Optimization parameters of PCL (Gesim)	27
3.1.2 Optimization parameters of PCL(Sigma – Aldrich)	29
3.1.3 Temperature measurement	31
3.2 Surface modification with alkaline hydrolysis treatment	32

3.3 Magnetic nanoparticles morphology	35
3.4 PCL melt electrowritten scaffolds with MNPs and Si-MNPs coating	35
3.5 Release of MNPs and Si-MNPs in medium	38
3.6 Mechanical strength test	39
3.7 Antioxidant Activity	40
3.8 Antibacterial Activity	40
3.9 Biological Activity	41
3.9.1 Cytotoxicity analysis – Indirect study with MG-63 osteoblast-like cells	41
3.9.2 Cell proliferation analysis – Direct study with MC3T3-E1 pre-osteoblast cells	43
4 Chapter 4 - Conclusion and future development	46
5 References	50

1. Introduction

1.1 Bone Cancers

Bone cancers are characterized by pain and bone destruction. The main treatments currently adopted are surgery, chemotherapy, and radiation therapy. However, in some cases, surgical resection is not able to completely remove tumor cells, with the consequence of recurrence and metastasis. Radiotherapy is not able to treat osteosarcoma and chemotherapy has important side effects. Moreover, bone defects caused by surgery should be repaired using biomaterials. For these reasons, the development of innovative biomaterials is essential for the treatment and therapy of bone cancer [1].

1.1.1 Osteosarcoma, Ewing sarcoma, Chondrosarcoma [2-4]

Osteosarcoma, Ewing sarcoma, and Chondrosarcoma are the main types of primary bone cancer. These neoplasms account for less than 1% of all cancers diagnosed each year but are significantly lethal.

Osteosarcoma is the principal bone cancer, it is a child and young adult illness (the third most common cancer in children), with a small increase in 60 years older people. Osteosarcoma originates from malignant primitive mesenchymal cells that differentiate into osteoblasts, which produce a malignant osteoid matrix. Osteosarcomas can occur in any bone but classically develop in the metaphyses of long bones. The areas where it most frequently develops are the distal femur, proximal tibia and proximal humerus. Osteosarcomas tend to appear at the age and location where bone growth is most active and when cells are vulnerable to mutations because the metaphysis of a bone contains the growth plate, which is responsible for active bone formation and elongation (*Fig.1*). Moreover, it grows quickly, occupying a large area of bone, which cannot repair itself. Osteosarcoma can metastasize and usually, its metastasis occurs in the lungs or other bones.

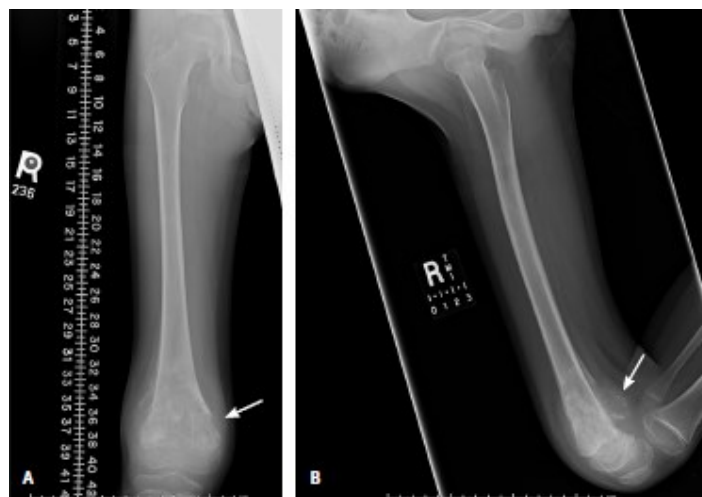


Figure 1. Radiographs of the distal femur of an eight-year-old boy with distal thigh pain and swelling who fell two days previously. (A) Anteroposterior view shows a sclerotic lesion with significant periosteal reaction. (B) The lateral view demonstrates posterior soft tissue tumor involvement. Biopsy of the lesion confirmed high-grade osteosarcoma [2].

The second most common bone cancer is Ewing sarcoma, which manifests in children and adolescents. Its cell origin is unknown, but recently it has been hypothesized it derives from primitive stem cells, and the degree of malignancy depends on the stage of stem cell arrest during differentiation. Ewing sarcoma has similar characteristics to osteosarcoma. The principal difference is the anatomic location of the development, which is the pelvis, long bones, diaphysis, and scapula for Ewing sarcoma.

Chondrosarcoma is a bone cancer that produces cartilage. It typically affects 40 years older adults and it usually appears in the central skeleton.

1.1.2 Principal bone cancer treatments [1-2]

Surgery and chemotherapy are the principal treatments for osteosarcoma. Neoadjuvant chemotherapy, followed by surgical resection and adjuvant chemotherapy is the main treatment for osteosarcoma. Radiation therapy is less effective and is rarely used. People with non-metastatic disease who survive beyond five years following treatment account for 70%. Limb amputations are still necessary for some expansive tumors.

For Ewing sarcoma, radiation therapy is used when surgery is not possible due to the location or size of the tumor, when there is a neurological compromise due to spinal tumors, and for lung metastases. Surgery is typically preferred because excisions with clear margins have improved survival rates in Ewing sarcoma. It is also believed that long-term radiation retards bone growth in childhood, and they are also associated with the development of subsequent neoplasms.

Chondrosarcoma is generally resistant to chemotherapy because the malignant cartilage cells have limited vascular connections, which make the administration of chemotherapeutic agents ineffective. The main treatment is always surgical resection, while radiation therapy is used when adequate surgical margins cannot be achieved.

1.2 Biomaterials for bone tumor therapy [1, 4]

Even if surgery, chemotherapy, and radiation therapy are the main treatments for bone cancer, surgery often does not remove the whole tumor, which causes the appearance of metastases, and chemotherapy often does not solve the problem of metastases. The result is a high mortality rate for bone cancer and most of the patients die from lung metastases.

Thanks to the development of bionanotechnology, there are new advanced treatment opportunities for bone cancer therapy. Nanotechnologies are useful for regenerative medicine due to multifunctional, theranostic, and stimuli-responsive biomaterials [5]. Biomaterials are biocompatible materials to be implanted in the human body to replace or repair organs or tissues, but also for diagnosis and therapy [1, 6].

For example, chemotherapy uses drugs with a lot of side effects (liver dysfunction, bone marrow suppression, heart toxicity) due to systemic delivery. New treatment methods based on biomaterials can decrease the side effects, by using a selective and local delivery [4].

An emerging treatment for bone cancer is photothermal therapy, which destroys tumor tissue, by converting near-infrared (NIR) light into localized thermal energy. This therapy uses nanomaterials with strong NIR absorption as gold nanoparticles, copper nanomaterials, carbon nanomaterials. It is very useful for localized tumors thanks to the concentration of irradiation

in one region and for the limitation of deep penetration of heat without damaging other tissues or organs.

Among nanomaterials, there are also magnetic nanoparticles (MNPs) that are used for example for hyperthermia. This method uses heat as a cancer treatment, due to an external alternating magnetic field that makes the MNPs, into the tumor, rotate, and in this way, the temperature increases and kills cancer cells, which are more susceptible to heat than normal cells [7].

Moreover, there are also biomaterial scaffolds, that may be used for bone tissue regeneration, to fill the cavity due to surgical removal of the tumor, and also to treat the cancer. The main task of biomaterials for bone cancer therapy is to kill cancer cells and to help bone regeneration. The treatments can be divided in local or systemic administration. Local treatments can consist of biomaterials, such as 3D-printed scaffolds, hydrogels, microspheres, and nanoparticles; these scaffolds can match the bone defect area and can contain active molecules to stimulate bone regeneration. Systemic administration consists of bone-targeting nanoparticles for bone cancer therapy that inhibit bone reabsorption (Fig.2), stimulate bone growth, or release anti-cancer drugs.

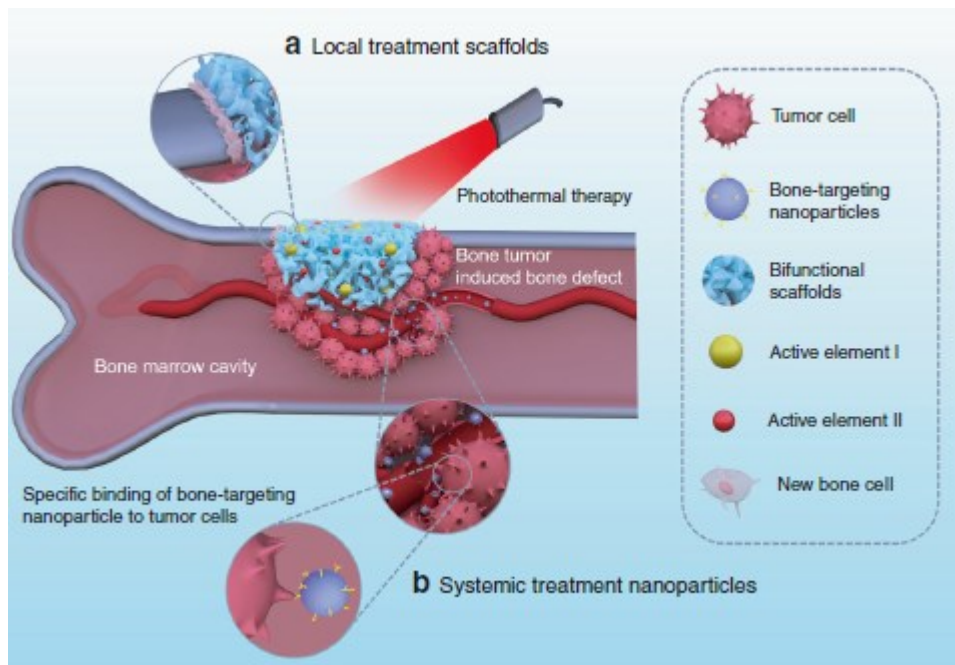


Figure 2. Bone tumor killed by (a) 3D-printed scaffold for local treatment, and (b) systemic treatment with administered nanoparticles penetrated blood vessels for photothermal therapy and bone regeneration [4].

To design scaffolds for bone cancer applications, it is important to consider properties like bioactivity, biocompatibility and biodegradability. Moreover, porosity, stiffness, and viscoelasticity could regulate cell adhesion, proliferation, and also osteogenesis differentiation. These scaffolds can also support cells physically and biologically [4].

For these reasons, the main aim of this thesis is to develop a PCL scaffold with magnetic nanoparticles coating, which should have good properties for bone cancer treatment.

1.3 Nanoparticles

1.3.1 Nanomedicine

Nanomedicine is the nanotechnology applied to the medical field, to create new treatments or drugs. A “nanomedicine” is a nano-formulated medicine.

Nanoparticles are materials with one dimension lower than 100 nm [8].

Nanoparticles are classified as [9]:

- Massive nanoparticles (*Fig. 3.a*), in which the particle material is massively formulated and the drug is dispersed within it;
- Nanocapsules (*Fig. 3.b*), in which the nanoparticle material forms the shell and it is hollow inside, so the drug can be dispersed both in the inner cavity and in the shell.
- Nanocomplexes (*Fig. 3.c*), massive particles with charge interactions. Therefore, negatively charged DNA or RNA nucleic acids are used, and positively charged polymers/materials balance the negative charge of the nucleic acid.

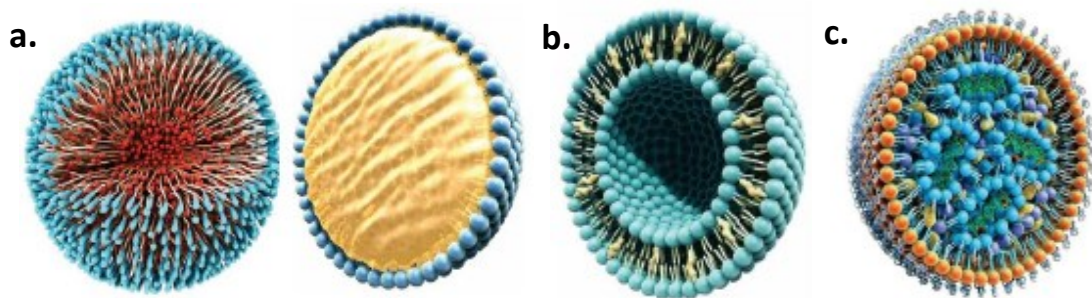


Figure 3. (a) massive nanoparticles, (b) nanocapsule, (c) nanocomplex [9].

Particles (*Fig.4*) can also be classified according to what they are composed of:

- Lipid nanocarriers, such as liposomes (nanocapsules that are hollow inside), stealth liposomes (particles that circulate in the blood without being recognized by the immune system), and solid lipid nanoparticles (massive particles);
- Polymer-based nanoparticles of different types;
- Inorganic nanoparticles, such as those metallic ones (iron oxide and gold nanoparticles) used more for imaging for contrast enhancement in magnetic resonance imaging (MRI), or hyperthermia of tumors. Those one based on silicon oxide, with nanopores into which the drug can be inserted. Quantum dots, which are mainly used to track particles in preclinical applications, i.e. animal tests and in vitro diagnosis;
- Viral nanoparticles, from the membranes of viruses by removing the infectious part and inserting the drug. They are used in vitro when one wants to modify the genome of the cell being studied;
- Drug-polymer conjugates: at the nano level, the drug is modified to bind to the polymer. They behave differently from the drug or polymer used alone.

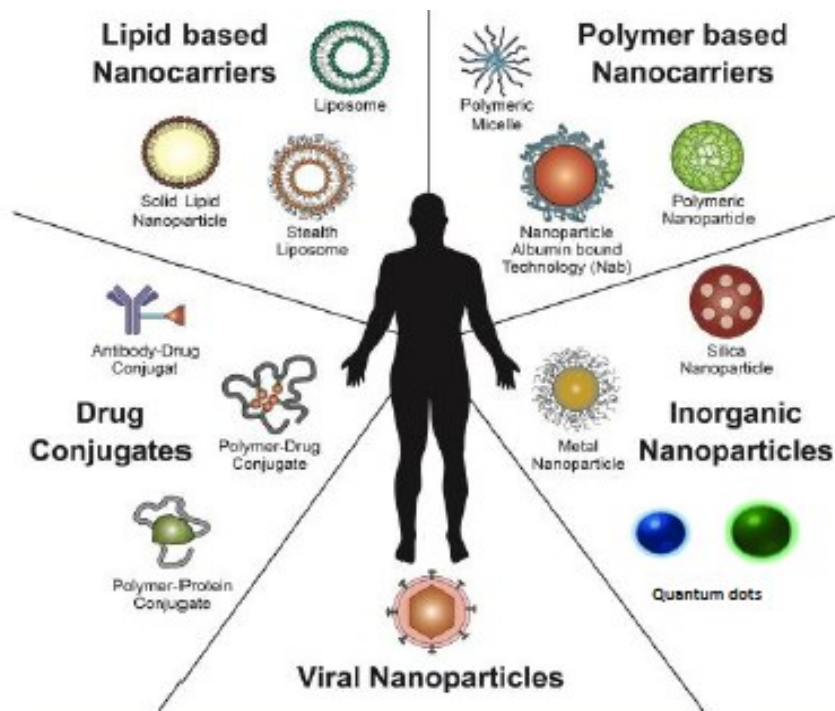


Figure 4. Different kinds of nanoparticle targeting [9].

Nanoparticles can interact with a specific target in different ways (Fig. 5):

- Passive targeting: which is related to tumor recognition, and takes advantage of the small particle size that permeates into the tumor mass;
- Active targeting: which is used not only for tumors. It requires specific recognition, so the particle must be modified to specifically recognize the cell and through ligand-receptor recognition permeate into it.
- Stimulus-mediated targeting: it sends the particles to the required site, but drug release only occurs through an external stimulus, or through a stimulus provided by the tumor itself. This is therefore referred to as intelligent stimulus or mediated stimulus.

Among the nanomedicines, we also find inorganic ones. They find applications in diagnosis and imaging, and if appropriately combined with drugs, can also be used for drug delivery or in tumor hyperthermia.

Inorganic nanomedicines are divided into:

- Metal nanoparticles: magnetic nanoparticles (iron oxide) and gold nanoparticles;
- Quantum dots: used for their ability to generate fluorescence;
- Nanobarcodes;
- Molecular beacons.

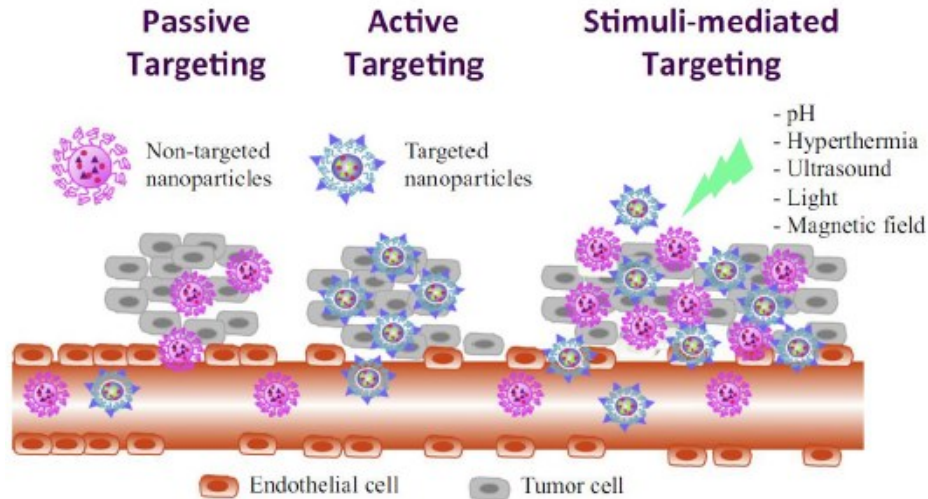


Figure 5. Classification of nanomedicines [9].

We now focus in particular on magnetic nanoparticles, one of the objects of study in this thesis.

1.3.2 Magnetic Nanoparticles

Magnetic (M) nanoparticles (NPs) are a class of nanoparticles that can be manipulated using a magnetic field (Fig.6). The most studied and used MNPs are Iron Oxide NPs, (IONPs), in particular, magnetite (Fe_3O_4) and maghemite ($\gamma\text{-Fe}_2\text{O}_3$). Usually, NPs consist of two components: a magnetic material and an organic component for stabilization and functionalization [9].

IONPs were used for in vitro diagnostics like contrast agents, and in the last years, they are developed also for drug delivery, MRI, magnetic hyperthermia, and biosensing. Magnetic IONPs are cheap to produce, biocompatible, physically and chemically stable, and environmentally friendly [10].

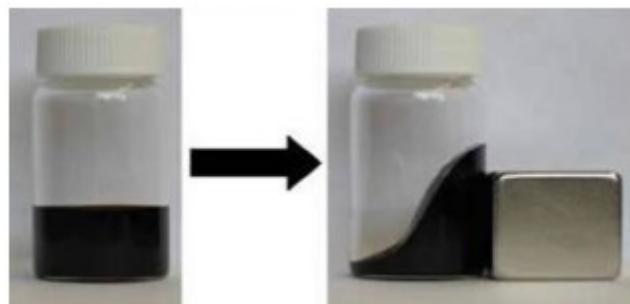


Figure 6. MNPs manipulated by a magnetic field (5).

1.3.2.1 Magnetic Properties

Many properties of MNPs are influenced by their size and shape. When the NPs size decreases, the surface-to-volume ratio increases, and the physical, chemical, and mechanical properties change, compared to the same materials at the bulk size [8]. The magnetic properties depend

on the morphology of IONPs, and in general, these NPs have superparamagnetic characteristics under the critical size of 50 nm [11]. The best size is below 15 nm [9-10].

Indeed, in large magnetic particles, there is a multi-domain structure and regions of uniform magnetization are separated by domain walls. If the MNPs size decreases below a critical diameter, MNPs can be composed of a single magnetic domain (each domain consists of moments of atoms aligned in one direction that give a net magnetization). If the temperature is above the blocking temperature (T_b), MNPs have a superparamagnetic behavior, and the magnetic moments of NPs fluctuate around the easy axes of magnetization. For this reason, each MNP has a large magnetic moment that changes orientation continuously. Thus, if a magnetic field is applied and MNPs are in a superparamagnetic state, they have a fast response to the magnetic field changes without residual magnetization and coercivity (the magnetic field required to bring the magnetization back to zero) [8]. The response type to the magnetic field and magnetization are measured from the hysteresis loops (M-H) and zero-field cooled/field cooled (ZFC/FC) curves. From the hysteresis loops, it is possible to obtain the saturation magnetization (M_s), the remanence magnetization (M_r), and the coercivity (H_c) (Fig. 7). If the IONPs are superparamagnetic, the M-H curve has no hysteresis [10]. Thus, MNPs with a superparamagnetic state behave as paramagnetic atoms with a giant spin. If the temperature is below the T_b , the thermal agitation is small and there are no fluctuations in the orientations of the magnetic moments of the NPs, which freeze in random orientations [8].

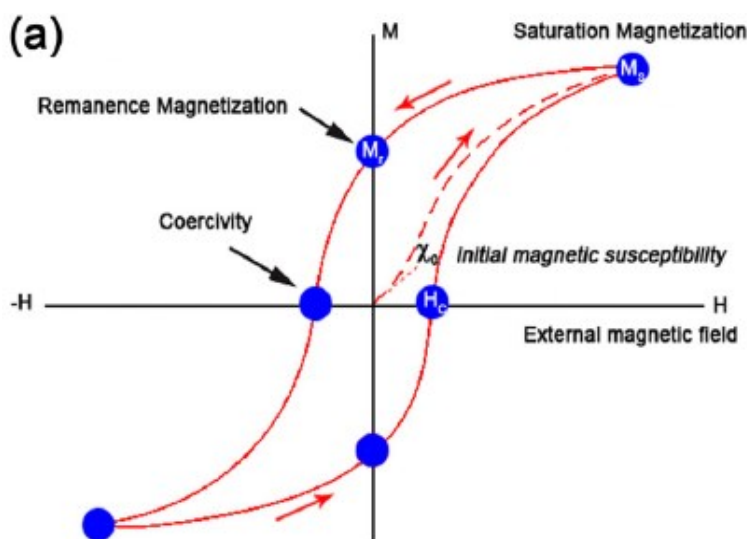


Figure 7. Schematic presentation of the hysteresis loops of IONPs [10].

1.3.2.2 Properties of Magnetic Nanoparticles for biomedical applications

The principal properties of NPs for biomedical applications are [8]:

- Biocompatibility, stability, and non-toxicity.
- Small size (10-50 nm): it is important to have superparamagnetic properties and to avoid particle aggregation when the magnetic interaction is reduced. Moreover, the small size means a bigger surface-volume ratio of the particles and reduced precipitation. Additionally, a small size consents the NPs, that are in blood circulation, to pass through the capillary system of organs and tissues, avoiding embolism.

- High saturation magnetization: it consents to control the movement of the NPs in the blood with a moderate external magnetic field, that can move the NPs near the targeted pathological tissue.
- Heat release: due to a high-frequency magnetic field, the magnetic moment of each nanoparticle may rotate to follow the field, and, in this way, heat may be generated. With more details, if there is the whole rotation of the NP, we are in the presence of Brownian relaxation in which the thermal energy is provided by the shear stress of the surrounding fluid. Otherwise, if the moment rotates but the NP remains fixed, we are in the presence of Néel relaxation, where the thermal energy is dissipated by the rearrangement of atomic dipole moments within the particle (*Fig. 8*). Both the mechanisms can be present at the same moment [12].

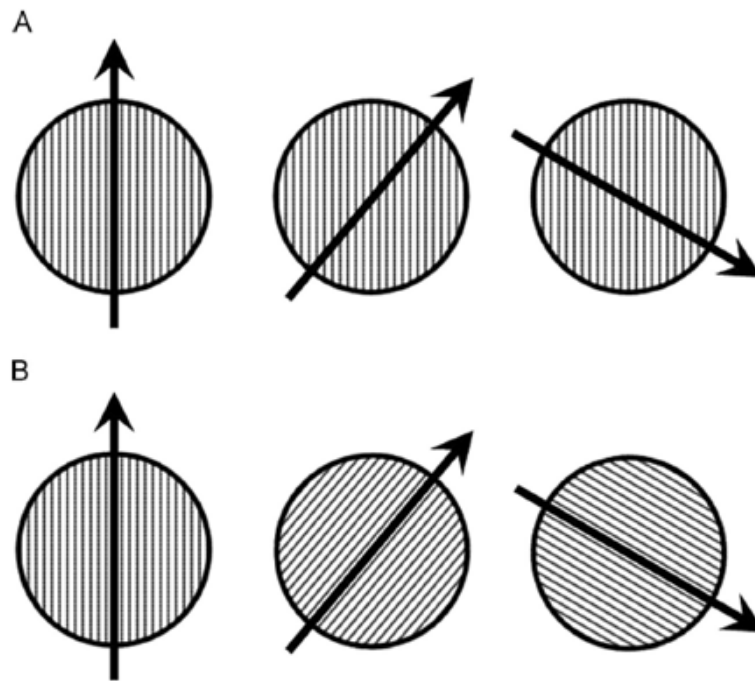


Figure 8. (a) Néel rotation: magnetic moment rotates with respect to the main axis of magnetisation, nanoparticle remains fixed, (b) Brownian rotation: magnetic moment remains fixed with respect to the main axis of magnetisation, nanoparticle rotates [12].

1.3.2.3 Synthesis of Magnetic Nanoparticles

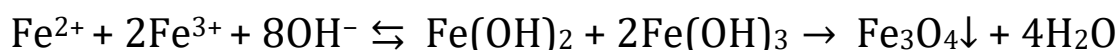
For the synthesis of magnetic nanoparticles in the biomedical field, it is important to control the particle size, shape, and surface structure. The main methods to produce nanoparticles (*Table 1*) are co-precipitation, micelle synthesis, thermal decomposition and reduction, hydrothermal and solvothermal synthesis, sol-gel synthesis, microemulsion, ultrasound irradiation, and biological synthesis [8, 10].

The synthesis method used for this project is co-precipitation. It is the most common method and consists of mixing ferric and ferrous ions in a 1:2 molar ratio in basic solutions at room temperature or elevated temperature.

Method	Reaction and conditions	Reaction temp. [°C]	Reaction period	Size distribution	Shape control	Yield
Co-precipitation	Very simple, ambient	20–150	Minutes	Relatively narrow	Not good	High/scalable
Thermal decomposition	Complicated, inert atmosphere	100–350	Hours-days	Very narrow	Very good	High/scalable
Hydro- or solvothermal synthesis	Simple, high pressure	150–220	Hours-days	Very narrow	Very good	High/scalable
Sol-gel and polyol method	Complicated, ambient	25–200	Hours	Narrow	Good	Medium
Microemulsion	Complicated, ambient	20–80	Hours	Narrow	Good	Low
Sonolysis or sonochemical method	Very simple, ambient	20–50	Minutes	Narrow	Bad	Medium
Microwave-assisted synthesis	Very simple, ambient	100–200	Minutes	Medium	Good	Medium
Biosynthesis	Complicated, ambient	Room temp.	Hours-days	Broad	Bad	Low
Electrochemical methods	Complicated, ambient	Room temp.	Hours-days	Medium	Medium	Medium
Aerosol/vapor methods	Complicated, inert atmosphere	>100	Minutes-hours	Relatively narrow	Medium	High/scalable

Table 1. Summary of methods to produce MNPs [10].

The chemical reaction is:



The nucleation of Fe_3O_4 is easier when the pH solution is lower than 11, while the growth of Fe_3O_4 nucleus is preferred when the pH is higher than 11.

This method has several advantages, like gram-scale production.

Anyway, the size, shape, and composition of the MNPs depend on the experimental parameters, for example, Fe(II)/Fe(III) ratio, the types of iron salts (chlorides, perchlorates, sulfates, nitrates, etc), pH value and ionic strength of the medium.

This method is one of the successful techniques to synthesize MNPs, but there are also negative aspects, such as the use of a strong base for the reaction process [10].

1.3.2.4 Application of Magnetic Nanoparticles in biomedical field

The main applications of MNPs in the biomedical fields are [8-10]:

- Magnetic hyperthermia: it uses an external electromagnetic field to allow the heat release by MNPs up to about 43°C; cancer cells are more sensitive to heat than healthy cells and can be destroyed preserving healthy cells. Moreover, tumors have a disorganized blood system, which does not allow them to release heat quickly. Thanks to the blood vessels, the NPs are able to penetrate the tumor cells. Through the external alternating magnetic field, the MNPs begin to rotate, generating localized heat with a temperature of 43°C, which kills the cells. This treatment is promising because [62]:
 - a. It is a non-invasive way to increase the cell temperature to a therapeutic level
 - b. MNPs can be seen from MRI, so it is possible to combine diagnostic and therapeutic approaches in one kind of particle
 - c. The nanoparticles may be functionalized with molecules and drugs, thus, hyperthermia could be combined with other treatments, for example, chemotherapy or radiotherapy.
- Drug and gene delivery (*Fig. 9*): nanoparticles may be able to load bio-therapeutic agents and use them in biomedical applications, such as cancer diagnosis and therapy [6]. MNPs with a coating may be functionalized with several molecules such as drugs, nucleic acids, carboxylic groups, or antibodies. These drug-loaded MNPs are used as magnetic vectors. They are injected intravenously and directed towards the site of interest through an external magnetic field.
- MRI contrast agents (CA): MRI is an imaging technique that consents to see soft-tissue contrast and safe levels of radiation. Tissue contrast can be increased with the use of CA,

which decreases longitudinal (T1) and transverse (T2) relaxation times. MNPs generate significant susceptibility effects in T1 and T2 contrast at low concentrations, so they are used as CA. Moreover, MNPs can be delivered to the targeted site using a magnetic field. Additionally, MNPs can be used in MRI for in vivo cell tracking to observe biological processes.

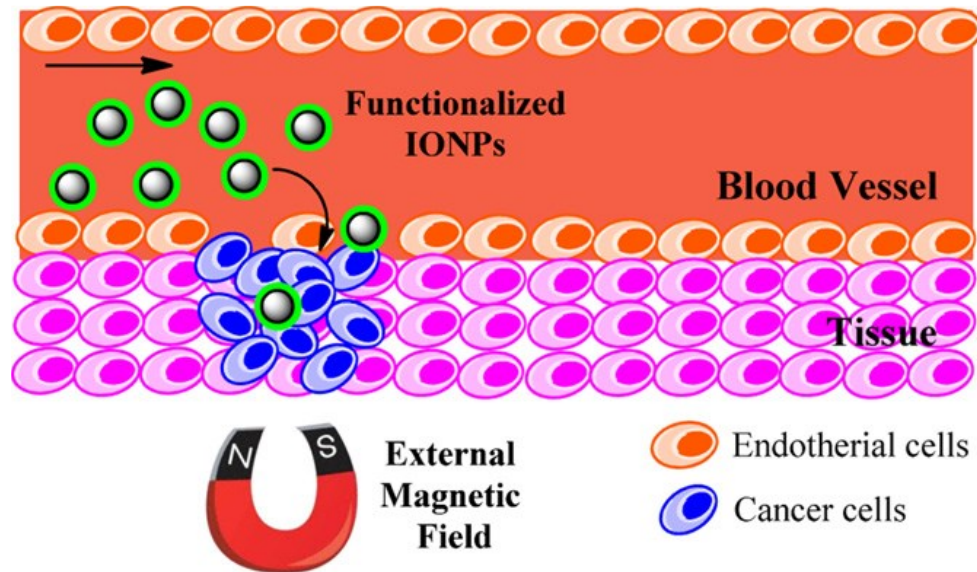


Figure 9. Schematic representation of MNPs-based drug delivery system: these magnetic carriers concentrate at the targeted site, due to the external magnetic field. Then, drugs are released from the MNPs [10].

1.3.2.5 Core-shell Magnetic-Silica Nanoparticles

MNPs in the size range are unstable for long periods, which manifests itself in different ways:

- loss of dispersibility: small NPs tend to aggregate and form large particles to reduce surface energy;
- loss of magnetism: bare MNPs have high chemical activity, so they are easily oxidized in air, particularly Fe_3O_4 and $\gamma\text{-Fe}_2\text{O}_3$.

Thus, it is necessary to create a protective shell to stabilize the MNPs, during or after the application. In the biomedical field, it is important to disperse the NPs in water, because biological media are usually aqueous solutions [6, 10].

Moreover, the coating is important for the stability of MNPs, which, otherwise, could precipitate due to gravitational force.

The coating is usually composed of organic materials such as polymers (polyvinyl alcohol (PVA), polyethylene glycol [PEG], etc. [8]), or inorganic materials such as carbon, silica, gold, or metal oxides [13].

It has been demonstrated that MNPs with superparamagnetic behaviour coated with a silica shell may be used in biomedical applications such as imaging, contrast agents, and drug targeted therapy [6].

In this project an inorganic material was used, in particular, a silica coating was developed. The silica layer can screen the magnetic dipolar attraction between MNPs, thus, this coating can increase the MNPs dispersion in solution [10]. Moreover, the silica coating enhances the

stability of MNPs and protects them from oxidation [13], and also provides many -OH groups, which can be bound to other biomolecules, drugs etc. [14].

Melt – Electrowriting

1.4.1 Melt-Electrowriting Technique

One of the most important methods for biomedical applications, such as biomaterials, tissue engineering, or biofabrication is the use of additive manufacturing (AM) because it could realize patient-specific designed scaffold. Melt electrowriting (MEW) is an emerging high-resolution AM technology that can print small well-interconnected porous structures, with a pore size suitable for tissue engineering (TE) applications. In particular, it can produce micro and nano fibers at micrometer or nanometer scale, useful to replicate the tissue microarchitecture of the human body due to their size smaller than cell size. This process is also solvent-free, so it is ideal for application in bone cancer and bone tissue engineering [15-17].

The MEW device is composed of a printing head and a heating system that melts the material inside the syringe (usually the material is a polymer). The melted polymer is delivered to a metal nozzle. Thanks to a delivery system, such as air pressure, and thanks to a potential difference between the nozzle and the collector, the extrusion of the polymer through the nozzle is possible. The electric field attracts the extruded material toward the collector while enabling the precise deposition of continuous strands in a layer-by-layer manner [15, 18]. The voltage is useful also to prevent Raleigh-Plateau instabilities [19]. The MEW head is controlled by a computer-aided translating system to print the designed scaffold. The electric field consents to concentrate the fluid drop charges in the closest point to the collector. The beginning of the jet and the fluid on the tip of the nozzle is called Taylor cone. When the Taylor cone is full of melt polymer, the polymer starts to drop, forming a thin column. Then, the polymer touches the collector and the direct-writing starts. The MEW jet depends on the applied voltage, collector distance, temperature, flow rate to the nozzle, air pressure, and melt viscosity and several minutes are necessary to start (*Fig. 10*).

Due to the printing parameters, it is possible to have fibers with different diameters and to create scaffolds, and porous structures used in the biomedical field. These porous scaffolds can promote cell infiltration and growth [16].

Another important parameter is the cartridge speed, which consents to deposit the material as straight lines if the speed is higher than the critical translation speed (CTS) of the melt polymer, which corresponds to the speed of the jet and the collector [15, 19].

Thanks to MEW, the result is uniform direct-written scaffolds with high porosity and fiber diameter ranges of 2-50 μm [20].

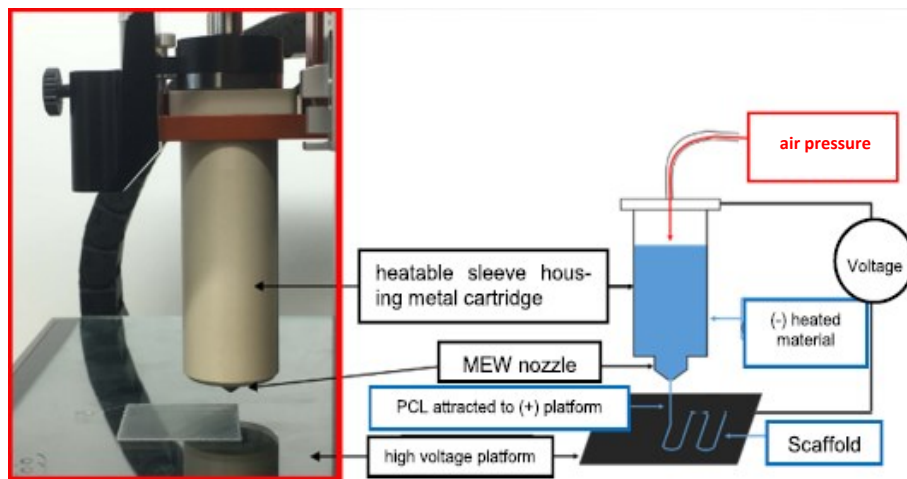
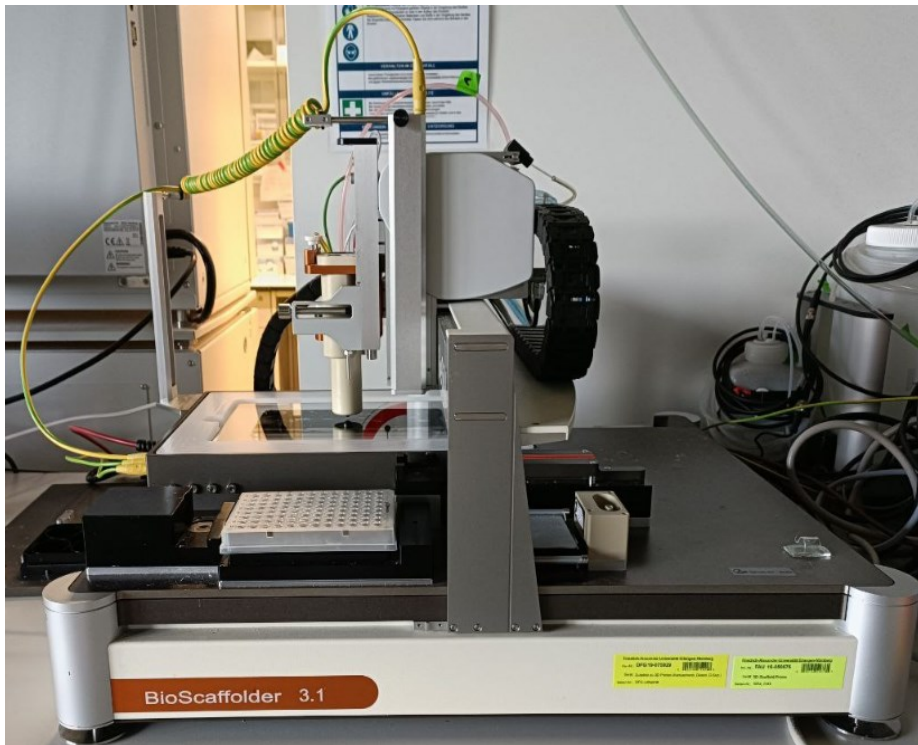


Figure 10. MEW system (top), heating cartridge (bottom, on the left) and working diagram (bottom, on the right) [18].

1.4.2 Polycaprolactone

Usually, materials used in MEW are polymers with a low melting point, for example, one of the most used is polycaprolactone (PCL). PCL is a semicrystalline, biocompatible, and biodegradable polyester, with mechanical strength and low cost. It is easily processable via MEW thanks to its low melting point temperature of 58–60°C and a glass transition temperature (T_g) of approximately -60°C [21], its high thermal stability, and its rapid solidification. PCL is approved by Food and Drug Administration (FDA) for clinical use, and it has a slow degradation rate up in years, so it is very used in biomedical applications [15, 18, 22]. The problem of PCL as a biomaterial is its hydrophobicity, which can cause handling issues in cell culture media. To solve this problem, usually, a surface modification on PCL is done, such as coating with molecules of conductive materials, functionalization with bioactive groups, or, for example, alkaline hydrolysis treatment, like in my thesis project.

1.4.3 PCL scaffold with MNPs coating in bone cancer applications

Although with the MEW we can fabricate scaffolds with properties required for cell ingrowth and tissue vascularization, until now, only pristine thermoplastic fibers, such as PCL, have been fabricated. Pristine polymer scaffolds have bio-inert behavior, so they are not ideal for TE applications. In bone regeneration applications, this means a lack of osteoinductivity which can delay or even prevent osteogenesis [16].

For this reason, in my thesis project, it was decided to perform an alkaline treatment that allows the exposure of the -OH and -COOH groups, making the scaffold more hydrophilic. This results in greater adhesion by MNPs and Si-MNPs when the coating is carried out.

The idea is the development of these scaffolds with MNPs and Si-MNPs for bone cancer applications (*Fig. 11*). In particular:

- Targeted drug delivery: thanks to an external magnetic field, we can direct the particles released by the scaffold into the cancer cells; moreover, a magnetic scaffold may be an attraction platform for magnetic carriers of growth factors, thus can enhance magnetic drug delivery in bone regeneration [5];
- Tissue stimulation: after the surgery to remove bone cancer, we can use our scaffold in the bone defect to stimulate bone regeneration thanks to MNPs and Si-MNPs; indeed, for example, it was demonstrated that MNPs with a silica shell has good magnetic and bioactive properties and it may be used as a filler for PMMA-based bone cements, to obtain multifunctional stimuli-responsive composite bone cements for the treatment of bone tumors [23]. Moreover, scaffolds with MNPs may attract stem cell migration and growth factors in the bone, due to a magnetic field that can control drug release and biomolecule activation, promoting bone regeneration [24].
- Hyperthermia: it may be used an external alternating magnetic field to rotate the MNPs and increase the temperature to over 43°C to kill the residual cancer cells in the bone tissue [5].

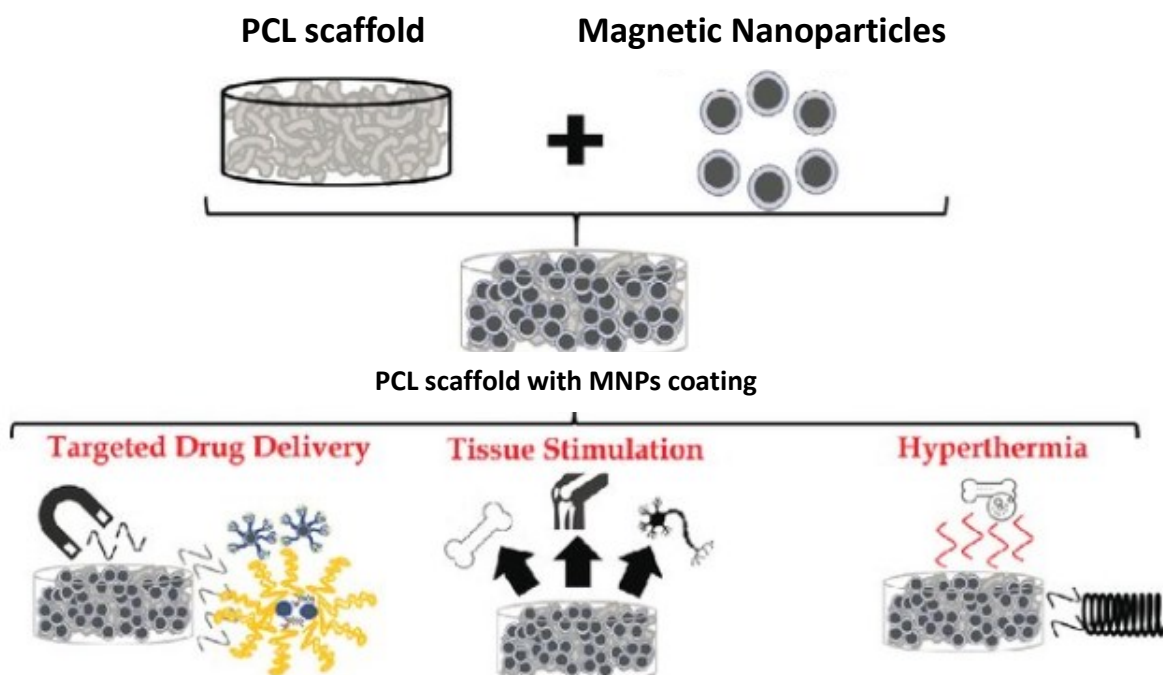


Figure 11. Bone cancer applications of PCL scaffold with MNPs or Si-MNPs coating.

2. Materials and Methods

2.1 Materials

The materials used for the MEW scaffolds are PCL from the printer company Gesim (Germany) and a commercial PCL (Mw=45 kDa) purchased from Sigma Aldrich (Germany). For the alkaline hydrolysis treatment were used Sodium hydroxide pellets for analysis (NaOH) from EMSURE (Germany), ethanol from Laborhaus Scheller GmbH & Co KG (Germany).

The materials used for nanoparticles are: Iron(II) chloride tetrahydrate ($\text{FeCl}_2 \cdot 4\text{H}_2\text{O}$), Iron(III) chloride esahydrate ($\text{FeCl}_3 \cdot 6\text{H}_2\text{O}$), ammonium hydroxide (NH_4OH), Citric Acid (CA), Tetraethyl orthosilicate (TEOS) purchased from Sigma-Aldrich.

For the antioxidant activity, it was used DPPH (2,2-diphenyl-1-picryl-hydrazyl-hydrate) from Biomol GmbH (Item number: Cay14805-100, Hamburg, Germany), methanol (34860), from Sigma Aldrich (Darmstadt, Germany).

Materials used for cell culture studies are the following: Fetal bovine serum (FBS; F2442), MG-63 osteoblast-like cell line (86051601-1VL), and M3T3-E1 pre-osteoblast-like cell line () were purchased from ThermoFisher Scientific (Schwerte, Germany).

Dulbecco's modified Eagle's medium (DMEM, 31885-023), Minimum Essential Medium α (MEM- α , 12571063), Phosphate buffered saline (PBS), Dulbecco's phosphate buffered saline (DPBS), and penicillin/streptomycin (PS, 15140-122) were purchased from Gibco - Thermo Fisher Scientific (Schwerte, Germany). α Glutamin and Trypsin were ordered from ThermoFisher Scientific (Schwerte, Germany).

Cytotoxicity was analyzed with WST8 purchased from Sigma Aldrich (Germany). For the cell proliferation was used WST8 Assay Kit ordered from Sigma Aldrich (Germany).

The microorganism strains of *Staphylococcus aureus* (ATCC25923) and *Escherichia coli* (ATCC25922) were used as model organisms for the determination of antibacterial activity. Luria/Miller agar (X969.1) and lysogeny broth medium (Luria/Miller, 6673.1) were supplied by Carl Roth GmbH (Karlsruhe, Germany).

Materials used for fluorescent cell staining are DAPI staining solution, Calcein AM, and Rhodamine phalloidin were purchased from Thermo Fisher Scientific (Schwerte, Germany).

For pH measurements: Buffer solution pH 7.00 ± 0.02 (20°C) and pH 4.00 ± 0.02 (20°C) ordered from Roth GmbH + Co (Germany), Dulbecco's modified Eagle's medium (DMEM, 31885-023), and Dulbecco's phosphate-buffered saline (PBS, no calcium, no magnesium, 10010023), ThermoFisher Scientific (Schwerte, Germany).

2.2 Methods

2.2.1 Preparation PCL

The MEW used to produce scaffolds is a Gesim Bioscaffolder 3.1 (Fig 12). The material used was PCL in pellet, which was melted inside the MEW cartridge in a heating oven with a constant temperature of 60 °C.

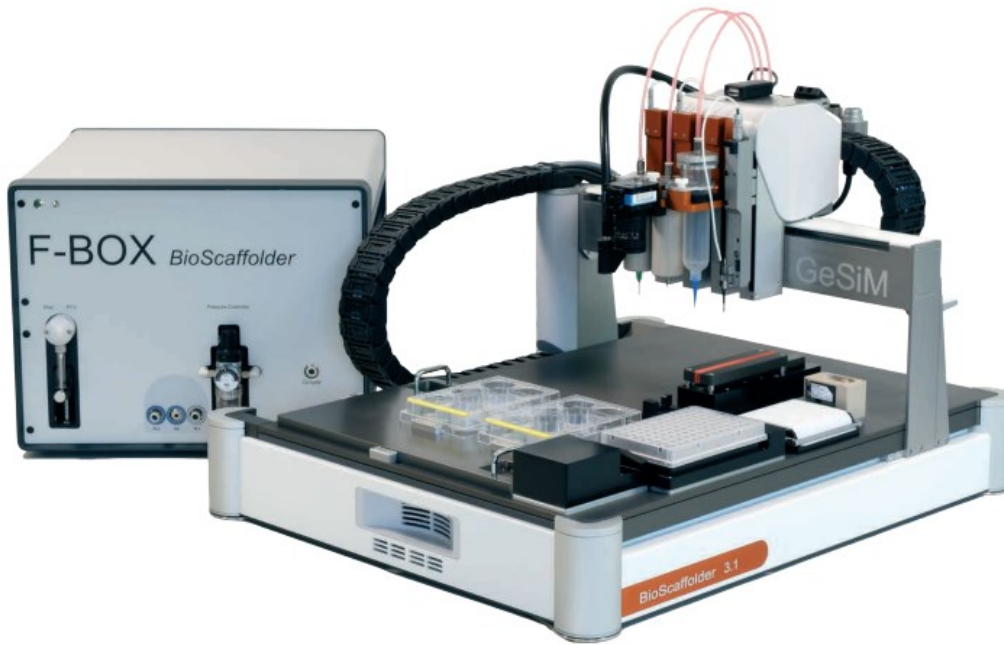


Figure 12. Gesim Bioscaffolder 3.1 Melt Electrowriting printer [25].

2.2.2 Melt electrowritten scaffold

2.2.2.1. MEW scaffold parameters

The cartridge with melted PCL was located in the MEW and the device was switched on. Then, the cartridge was raised to a temperature of 85 °C and it was waited for 1 h before starting to print. The scaffold parameters were set via the G-Code program from the printer. After different tests, the parameters chosen to print PCL from the printer were: temperature of 75°C, pressure of 200 kPa, distance between collector and nozzle of 1 mm, speed of the cartridge 25 mm/s, voltage 6 kV, infill distance 0.450 mm, stand height 0.250 mm, 12 layers.

Then, the material had to be changed as the PCL supplied by the company with the printer was not for sale. Therefore, started using PCL (Sigma – Aldrich). The parameters to print PCL from Sigma Aldrich were temperature of 85°C, pressure of 255 kPa, distance between collector and nozzle of 0.350 mm, speed of the cartridge 28 mm/s, voltage 4 kV, infill distance 0.325 mm, stand height 0.100 mm, 12 layers.

In both cases, the obtained samples were square and 13 mmx13 mm in size.

2.2.2.2 Temperature measurement

A visual IR thermometer (Fluke) was used to detect the real temperature in the middle of the cartridge and on the tip. The measurements were done at different time points after 1 h at 85 °C from the software (20 min, 40 min, 100 min, 160 min). This analysis was done for 4 days, then average \pm standard deviation values were measured.

2.2.3 Surface modification with alkaline hydrolysis treatment

PCL is a hydrophobic material and to have good adhesion of nanoparticles and cells, it is necessary a surface modification [26]. It was chosen to modify the PCL scaffolds with alkaline hydrolysis treatment, using NaOH in water (0.5 M). With this method, the OH⁻ groups could react with C=O, C-O and C-O-C functional groups of the polymer surface, remove the short segments of the polymeric chains and it is possible to obtain the exposure of groups -OH and -COOH useful to have a more hydrophilic material [27], so, to increase the cells and particles adhesion. Briefly, after sterilizing the samples by soaking them in ethanol for 15 min, they are dried and immersed in the NaOH solution, where they are stirred using a magnetic stirrer. Samples are taken from the solution after 1 h, 2 h, and 3 h and dried overnight under fume hood. To detect the surface modification, samples were analyzed by ATR-FTIR, SEM, contact angle measurement, and antioxidant activity.

2.2.4 Magnetic Nanoparticles Coating

2.2.4.1 Magnetic Nanoparticles preparation

Magnetic nanoparticles were synthesized at the Polytechnic of Turin, according to this paper by Antonia Follenzi et al [13]. To synthesize the MNPs, the chemical co-precipitation method in water was used. FeCl₂*4H₂O (2.04 g of FeCl₂ in 100 mL of water) and FeCl₃*6H₂O (2.6 g of FeCl₃ in 100 mL of water) solutions were mechanically mixed in water (0.01 M) with a ratio of

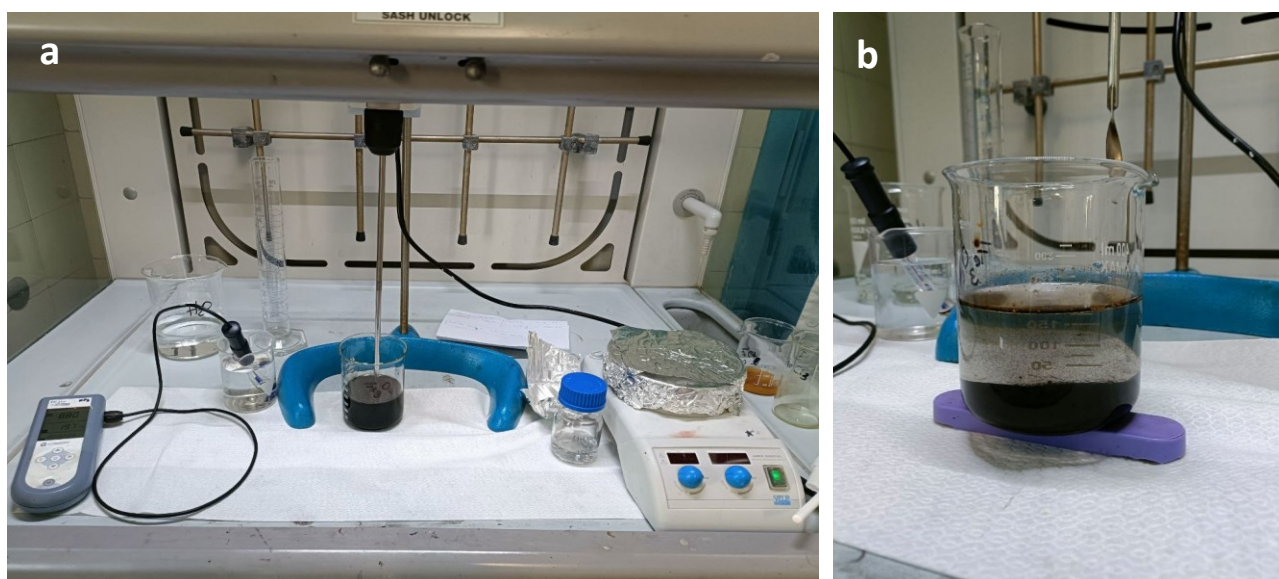


Figure 13. (a) A picture of FeCl₂/4H₂O and FeCl₃/6H₂O solutions mechanically mixed to obtain Fe²⁺/Fe³⁺ in a ratio of 1:2, and on the left the pH meter used; (b) MNPs on the bottom of the beaker, attracted by the magnet.

3:4, to obtain a stoichiometric ratio of $\text{Fe}^{2+}/\text{Fe}^{3+}$ of 1:2. The pH of the solution was increased up to 10 by adding NH_4OH drops (*Fig. 13 a*). The solution became black, and it was placed in an ultrasound bath for 20 min to allow the MNPs growth. After that, the MNPs were placed in a beaker and a magnet was used to attract them to the bottom (*Fig. 13 b*). Then the excess liquid was removed and two washes with bi-distilled water were carried out.

These nanoparticles have already been magnetically characterized in previous works [13, 28-29].

2.2.4.2 Citric Acid dispersion

Then, MNPs were suspended in a solution of citric acid (CA) to improve the dispersion of the nanoparticles in water. CA presents carboxyl groups, and at least one of them is exposed to the solvent, imparting a negative surface charge to the MNPs it covered. In this way, the MNPs repelled each other, and the dispersion is improved. Moreover, the presence of a carboxyl group as a surface ligand offered the possibility of developing bonds with other molecule linkers to facilitate precise targeting in biological systems [30]. After the last wash, an amount of 150 mL of MNPs solution was re-suspended in 180 mL of 0.05 M solution of citric acid (CA) [31]. Again, the pH was basified until 5.2, using NH_4OH drops. The suspension was located in an orbital shaker (KS 4000i control, IKA_) at 150 rpm, for 90 min at 80 °C, to allow the deprotonation of two carboxylic groups of CA and the bond to the OH groups exposed by MNPs. After the functionalization with CA, the MNPs were washed with Milli-Q water in an ultrafiltration device (Solvent Resistant Stirred Cells - Merck Millipore) (*Fig. 14*). This device was placed on a mechanical stirrer at a speed of 180 rpm and connected to an argon cylinder that provided 3 bar pressure to remove excess liquid. Then, MNPs were resuspended in bi-distilled water, and the pH was adjusted at 10.2, to have a better MNPs dispersion, due to the third carboxylic group deprotonation.

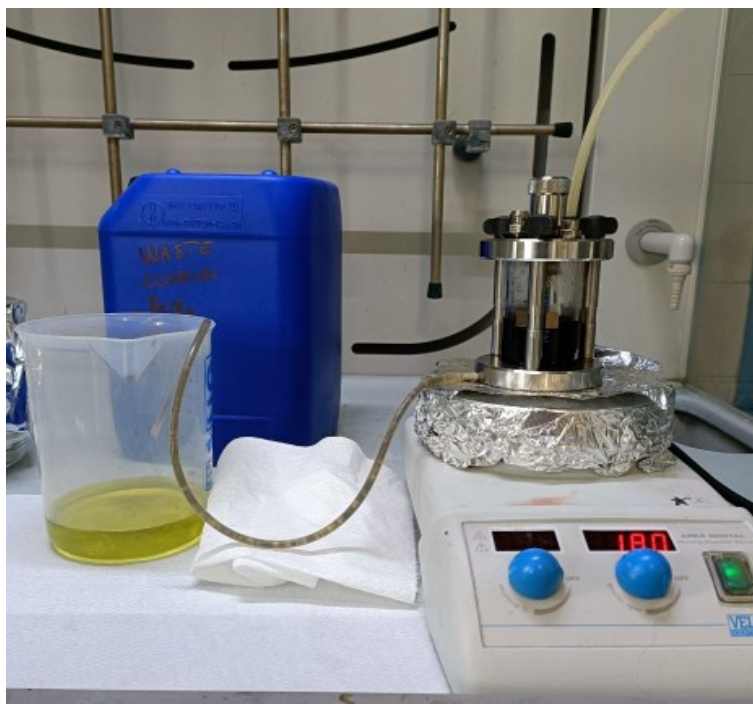


Figure 14. A picture of the ultrafiltration device placed on a mechanical stirrer at a speed of 180 rpm and connected to an argon cylinder that provided 3 bar pressure to remove excess liquid. The yellow liquid on the left is the NPs waste liquid.

2.2.4.3 Silica shell coating

Subsequently, the MNPs were coated with a silica shell (Si-MNPs) using the Stöber method [32]. This method is a chemical synthesis usually used to prepare silica nanoparticles with controllable growth and uniform size [6]. Briefly, the MNPs were ultrafiltrated, then dispersed in a solution of ethanol and bi-distilled water with a ratio of 4:1. A mixture of Tetraethyl orthosilicate (TEOS, as silica precursor), ethanol, and water (with an ethanol:water ratio of 1:1) was prepared and added to the MNPs + CA solution for 3 h at 25 °C and 150 rpm. After the 3 h, Si-MNPs were washed two times with bi-distilled water, using the ultrafiltration device. Finally, they were redispersed in water.

At the end, solutions of MNPs in water with a concentration of 9 mg/mL, MNPs + CA with a concentration of 5 mg/mL, and Si-MNPs with a concentration of 5 mg/mL were obtained.

2.2.4.4 PCL melt electrowritten scaffolds with MNPs and Si-MNPs coating

After the alkaline hydrolysis treatment, the PCL melt electrowritten scaffolds were coated with the nanoparticles. In particular, MNPs + CA, and Si-MNPs were used. Briefly, 1 mL of MNPs solution was mixed with 4 mL of CA solution (0.05 M). The same was done for Si-MNPs solution. Then, samples were immersed in the solutions. In particular, PCL – 1 h NaOH, PCL – 2 h NaOH, PCL – 3 h NaOH scaffolds were immersed in MNPs or Si-MNPs solution for 1 min and 3 min. In the beginning, it was tried also an immersion of 6 min.

2.2.5 Characterization

2.2.5.1 Surface morphology

The PCL scaffold microstructure was examined using a light microscope (Primo Vert, Carl Zeiss).

Scanning electron microscopy (SEM, AURIGA base 55, Carl Zeiss, Germany) was used to examine the scaffolds' nanostructure and to analyze the presence of MNPs and Si-MNPs on the surface of the fibers. According to this paper from A. Boccaccini and his group [33], the samples were coated with a thin layer of gold (Q150T Turbo-Pumped Sputter Coater/Carbon Coater, Quorum Technologies) before SEM analyses. Before SEM analysis, the samples were coated with a thin layer of gold (Q150T Turbo-Pumped Sputter Coater/Carbon Coater, Quorum Technologies). To measure fibers diameter and pore size from SEM images, the Image J analysis software (NIH, Bethesda, MD, USA) was used. In particular, an average of the fiber diameter was evaluated, by measuring at 50 random points for each sample.

All the SEM images were carried out by my technical supervisor Irem Unalan.

2.2.5.2 Surface chemistry

To identify the chemical structure of the scaffolds, the presence of PCL, MNPs, and Si-MNPs Attenuated total reflectance (ATR) - Fourier-transformed infrared spectroscopy (FTIR) (IRAffinity-1S Shimadzu) (*Fig. 15*) was used. The wavenumbers range of the infrared spectra was between 400 and 4000 cm^{-1} , with a spectral resolution of 4 cm^{-1} .



Figure 15. FTIR device (IRAffinity-1S Shimadzu).

The wettability of the scaffolds was analyzed with the contact angle meter (Drop Shape Analyzer, DSA 30, CA Measurement setup, Krüss GmbH, Hamburg, Germany), using a sessile drop method. According to this paper from A.R. Boccaccini et al [33], the samples were positioned on a glass slide for the test. The analysis consists of 8 μL of de-ionized water drops falling on the surface of the samples (Fig. 16). In particular, the water was dropped on different points of the same scaffold to have an average value of the contact angle measurement.

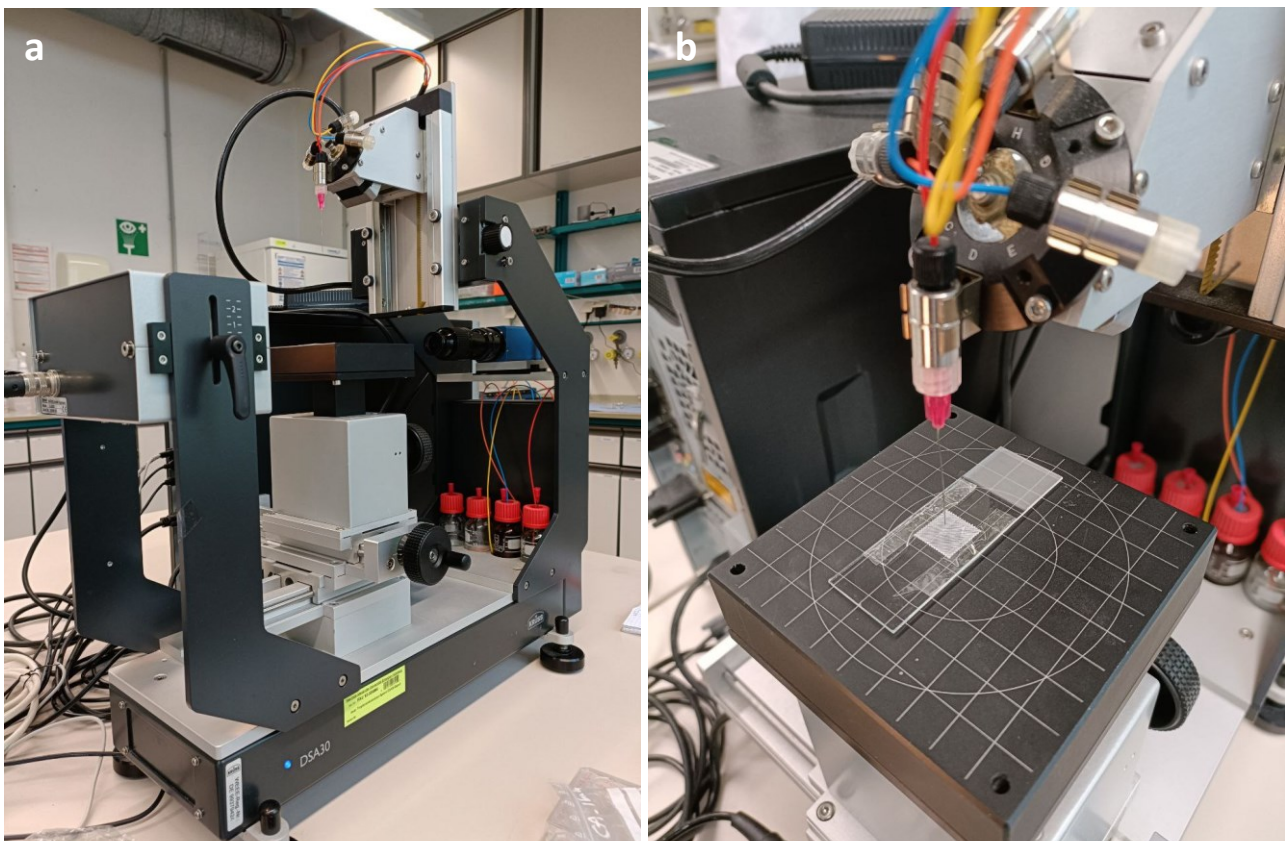


Figure 16. a) Contact angle meter (Drop Shape Analyzer, DSA 30, CA Measurement setup, Krüss GmbH, Hamburg, Germany). b) the sample on a glass slide for the analysis.

2.2.6 Release of MNPs and Si-MNPs in medium

Following the coating, it was planned to analyze whether the scaffold would release the nanoparticles into the medium or whether they remained attached. The adhesion of MNPs and Si-MNPs coating on the PCL scaffold with alkaline hydrolysis treatment was analyzed by incubating different samples in DMEM medium solution for 1 day and 7 days with a speed of 142 rpm and a temperature of 38 °C. After the set times, the samples were taken and washed with ultra-pure water three times and dried in incubator overnight. The pH medium was measured, and the samples were examined by ATR-FTIR and SEM to assess a possible release of nanoparticles.

2.2.7 Mechanical strength test

For the mechanical analysis, a uniaxial mechanical testing device (Instron 5967, Instron® GmbH, Germany) (Fig. 17) was used. In particular, scaffolds with only PCL, with PCL modified with alkaline hydrolysis treatment and with a coating of MNPs and Si-MNPs were analyzed. The samples had a width of 5 mm and a height of 13 mm. Briefly, a tensile test was carried out, with a speed of 1 mm/min, and a load cell of 100 N at room temperature. For each kind of sample, nine replicas were used and average \pm standard deviation values were measured.



Figure 17. (a) Uniaxial mechanical testing device (Instron 5967, Instron® GmbH, Germany), (b) the tensile strength analysis on the scaffold.

2.2.8 Antioxidant Activity

Free radicals are highly reactive chemicals with the potential to damage cells. They are created when an atom, or a molecule, gains or loses an electron and they are formed naturally in the body for a lot of cellular processes. However, at high concentrations, they can damage cells components, including DNA, proteins, and cell membranes. This damage to cells, especially to DNA, may be the cause of the development of cancer. Antioxidants are chemicals that interact with free radicals to neutralize them, thus preventing them from causing damage. Antioxidants are also known as “free radical scavengers” [62], and the research for new antioxidant molecules has greatly intensified. In particular, a study was carried out to study the antioxidant

activity of MNPs, with successful results [34]. For these reasons, it was chosen to analyze the antioxidant activity of these scaffolds.

For the antioxidant activity, a DPPH assay was used [35], to evaluate the free radical scavenging activity of different scaffold types. DPPH free radical method is an antioxidant assay based on electron-transfer that produces a violet solution in methanol. This free radical, stable at room temperature, is reduced in the presence of an antioxidant molecule, giving rise to colorless methanol solution. The use of the DPPH assay provides an easy and rapid way to evaluate antioxidants by spectrophotometry [65]. Each scaffold type was immersed in 2 mL of methanol solution overnight. After that, each sample with 0.5 mL of the methanol solution was reacted with 2.5 mL of DPPH radical solution (in the concentration of 0.04 mg/mL). After a 90 min incubation in darkness at room temperature, the absorbance was measured by UV-Vis spectroscopy (Analytik Jena SPECORD 40 from LabX device) at 517 nm. The methanol solution was used as blank, while DPPH solution was used as control.

The equation (*eq. 1*) used to determine DPPH radical scavenging activity is the following:

$$\text{DPPH radical scavenging activity (\%)} = \frac{\text{Absorbance of sample}}{\text{Absorbance of control}} * 100$$

Equation 1.

2.2.9 Antibacterial Activity

Bacteria may be linked with cancer for two reasons: they could cause chronic inflammation, which may lead to cancer, they could weaken the immune system, and they could produce carcinogenic bacterial metabolites [36-37]. Moreover, bacteria may also induce host cell DNA damage and thus interfere with host cell pathways involved in cell proliferation, apoptosis, and differentiation, increasing the likelihood of developing cancer [38].

Thus, the antibacterial activity was studied because it has shown that MNPs could offer antibacterial activity against both gram-positive and gram-negative bacteria [39, 40-42]. The antibacterial activity was done following this paper from A.R. Boccaccini group [33]. PCL, PCL – 3h NaOH, PCL – 3 min MNPs, PCL – 3 min Si-MNPs scaffolds were separately tested with *S.aureus* (Gram-positive) and *E. coli* (Gram-negative) bacteria. Briefly, a lysogeny broth medium at 37 °C for 24 h was used to prepare the bacterial suspensions for both bacteria stains. To analyze the cultivated bacteria, the optical density (OD) (600 nm, Thermo Scientific GENESYS 30, Germany) was used at 0.015. The scaffolds were sterilized by UV light irradiation for 30 min before being immersed in the lysogeny broth medium. Moreover, 20 µL of bacteria suspension was added. Then, all the scaffolds were incubated at 37 °C for 3 h, 6 h, and 24 h and they were analyzed at each time point at 600 nm OD.

The bacteria viability was measured with the following equation (*Eq. 2*):

$$\text{Relative viability (\%)} = \frac{\text{OD sample}}{\text{OD control}} * 100$$

Equation 2.

The lysogeny broth medium was used as a blank, while the bacterial cell suspension in the lysogeny broth medium was the control. The experiments were performed three times.

The antibacterial activity study was carried out by my technical supervisor Irem Unalan.

2.2.10 Biological Activity

2.2.10.1 Cell Culture

Cytotoxicity and cell proliferation were analyzed to understand if the samples had good cell viability.

In particular, the direct study analyzed cell growth in the samples, while the indirect study analyzed the cytotoxicity of the samples.

MG-63 osteoblast-like cells were used for the indirect contact method to analyze the cytotoxicity, while the cell proliferation was studied with M3T3-E1 pre-osteoblast-like cell line using the direct method.

For the indirect study, 14 cells split passage was used, while for the direct method the 11 cells passage.

MG-63 osteoblast-like cells were cultured in a solution of DMEM with 10% (v/v) FBS, 1% (v/v) PS, and incubated at 37 °C in a humidified atmosphere of 5% carbon dioxide (CO₂) atmosphere.

M3T3-E1 pre-osteoblast-like cells were cultured in MEM – α with 10% (v/v) FBS, 1% (v/v) PS, α – Glutamin 1% (v/v) and incubated at 37 °C in a humidified atmosphere of 5% CO₂ atmosphere.

The cell studies were carried out by my technical supervisor Irem Unalan and me.

2.2.10.2 Cytotoxicity

The cytotoxicity of PCL, PCL – 3h NaOH, PCL – 3 min MNPs, PCL – 3 min Si-MNPs scaffolds was analyzed using WST-8 cell proliferation assay kit, with the indirect contact method, like in this



Figure 18. Picture of the hemacytometer with cells that were counted looking through the microscope.

paper [43]. MG-63 osteoblast-like cells were cultured in a solution of DMEM with 10% (v/v) FBS, 1% (v/v) PS, and incubated at 37 °C in a humidified atmosphere of 5% carbon dioxide (CO₂) atmosphere. Then, cells count was done. Briefly, 100 µl of trypan blue and 100 µl of cells solution were mixed and placed in the hemacytometer (Paul Marienfeld GmbH & Co. KG) where the cells were counted looking through the microscope (Zeiss Primovert) (Fig. 18). Afterwards, the cells solution was centrifugated (Centrifuge 5804 – Eppendorf), to obtain the cells pellet, which was immersed in fresh medium. After that, MG- 63 cells were seeded in 6-well plates at a density of 4.5*10⁵ cells/well (1 mL of cells solution + 1 mL of fresh medium for each well) and incubated for 24 h. In the meanwhile, samples were sterilized with UV radiation for 1 h. After 24 h of cell incubation, the scaffolds were added to the well plates, in particular, one sample for each well, and re-incubated for another 48 h.

Thereafter, the cytotoxicity was measured by WST-8 assay. The medium was replaced with a solution of WST (1% v/v) in medium and the cells were incubated for another 3 h. Finally, the optical density of the solution was measured at 450 nm using a microplate reader (FLUOstar Omega - BMG Labtech).

The percentage of cell viability was calculated by the following equation (Eq. 3):

$$\text{Cell viability (\%)} = \frac{\text{Absorbance of sample} - \text{Absorbance of blank}}{\text{Absorbance of control} - \text{Absorbance of blank}} * 100$$

Equation 3.

WST was used as blank, while the MG-63 cells were the control. All samples were measured eight times.

2.2.10.3 Cell proliferation

M3T3-E1 pre-osteoblast-like cell line was used to analyze the cell proliferation with the direct method after 1 day and 7 days. M3T3-E1 pre-osteoblast-like cells were cultured in MEM – α with 10% (v/v) FBS, 1% (v/v) PS, α – Glutamin 1% (v/v) and incubated at 37 °C in a humidified atmosphere of 5% CO₂ atmosphere. As for the cytotoxicity study, cells count was done. 100 µl of trypan blue and 100 µl of cells solution were mixed and placed in the hemacytometer where the cells were counted looking through the microscope. Afterwards, the cells solution was centrifugated, to obtain the cells pellet, which was immersed in fresh medium. The study was done with a cell density of 10⁵ cells/µL. The cells with medium were placed in a well-plate with one sample for each well for 3 h. After this time, other fresh medium was put in each well and the samples were located in incubator. After 24 h, the samples were washed with PBS and half of the scaffolds were used to study the cell proliferation on the samples after 1 day, while the other half was immersed in fresh medium and placed in incubator for other 6 days, to analyze the cell proliferation after 7 days.

WST-8 assay was used to study the cell proliferation. The medium was replaced with a solution of WST (5% v/v) in medium and the cells were incubated for another 3 h. Then, the optical density of the solution was measured at 450 nm using the microplate reader.

The percentage of cell viability was calculated by the same equation (Eq. 3) of the cytotoxicity study, but now the blank is WST, while the control is the PCL scaffold.

2.2.10.4 Cell Morphology - Fluorescent cell staining

In both direct and indirect cell studies, the cell morphology on the samples was analyzed by fluorescence microscopy (DMI 6000B, Leica, Germany).

The samples with cells were washed with PBS. Then 1 mL of a solution of Calcein (C) (4 μ L) and medium was put in each sample. The samples were placed in incubator at 37°C at 5% CO₂ and in darkness for 45 min. After that, C was removed and the samples washed. Then, each sample was fixed with 1 mL of Fluo-FIX for 15 min in darkness. Afterward, the fixing solution was removed and the samples were washed again. Subsequently, 1 mL of a permeabilization solution was used in each sample in darkness. After 5 min, it was removed and 1 mL of phalloidin (P) (8 μ L) and medium solution was put in each sample. Then, the scaffolds were placed in incubator at 37°C at 5% CO₂ and in darkness for 45 min. Finally, the P was removed, the samples were washed and 1 mL of a solution of DAPI (D) (1 μ L) and medium was put in each sample for 5min. After removing D, scaffolds were washed and 3 mL of PBS was put in each sample. Then, the samples were stored in fridge at the temperature of 4 °C for 7 days in darkness.

3. Results & Discussion

3.1 Melt electrowritten scaffolds

The parameters of MEW which can be changed to obtain good scaffolds are temperature, pressure, voltage, distance between collector and nozzle, speed, infill distance, and stand height. According to the literature, the optimal temperature for PCL should be between 73 and 100 °C, the optimal pressure between 20 and 200 kPa, and the best voltage between 4.5 and 12 kV [17-18, 20, 44-48]. The fiber diameter depends on the pressure and the speed, the higher they are, the thinner the fibers will be [19], but also on the distance between collector and nozzle, as the distance increases, the pore size increases and the deposition of the material loses precision [18].

Therefore, several tests were carried out, varying one parameter per time, and keeping the others fixed, for both PCL (Gesim) and PCL (Sigma – Aldrich).

3.1.1 Optimization parameters of PCL (Gesim)

At the beginning, after reading the literature [17-18, 20, 44-48], it was chosen to start with some constant parameters and change one parameter per time, to find the optimal ones. At first, the chosen constant parameters were 85°C, 200kPa, distance of 1mm, speed 25 mm/s, infill distance of 0.450mm, and stand height: 0.250 mm, while voltage was tested at 5 and 6 kV, confirming 6 kV as the best (*Fig. 19 a, b*). Then, distances of 1 mm, 2 mm, 3 mm and 4 mm were evaluated (*Fig. 19 b, c, d, e*), with 1 mm being the optimal distance. The same was done with temperature (70, 75, 85, 90 °C) (*Fig. 19 f, g, h*) and the best one was 75 °C. At a temperature of 90°C, the sample was so delicate that it was destroyed when removing it from the collector. As can be seen from *figure 16 b*, at the beginning, a temperature of 85°C seemed good, but, after different tests, with this temperature, the results were not good anymore (*Fig. 19 h*), probably because at first the temperature had not yet reached 85 °C, the set temperature.

Finally, after these tests, the optimal parameters to print PCL (Gesim) were: temperature of 75°C, pressure of 200 kPa, distance between collector and nozzle of 1 mm, speed of the cartridge 25 mm/s, voltage 6 kV, infill distance 0.450 mm, stand height 0.250 mm, 12 layers (*Fig. 19 h – Fig. 20*). Then, fiber diameter and pore size of the final scaffold were measured by the software ImageJ. The fiber diameter was $44 \pm 1 \mu\text{m}$, while the pore size was $446 \pm 8 \mu\text{m}$ (x-axis) and $450 \pm 3 \mu\text{m}$ (y-axis).

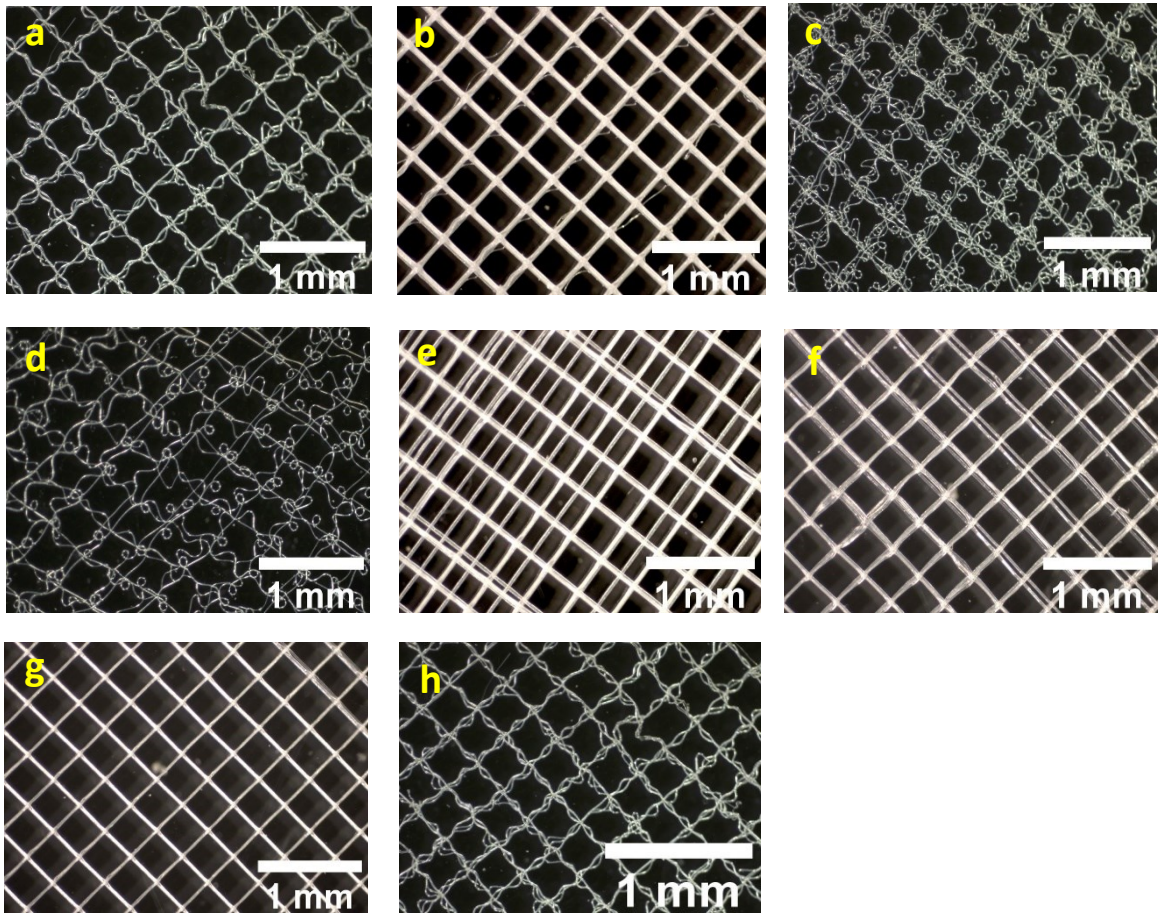


Figure 19. Microscope images 2X of PCL scaffolds with (a) 5kV, 1 mm, 85 °C (b) 6 kV, 1 mm, 85 °C (c) 6 kV, 2 mm, 85 °C (d) 6 kV, 3 mm, 85 °C (e) 6 kV, 4 mm, 85 °C (f) 6 kV, 1 mm, 70 °C (g) 6 kV, 1 mm, 75 °C, (h) 6 kV, 1 mm, 85 °C.

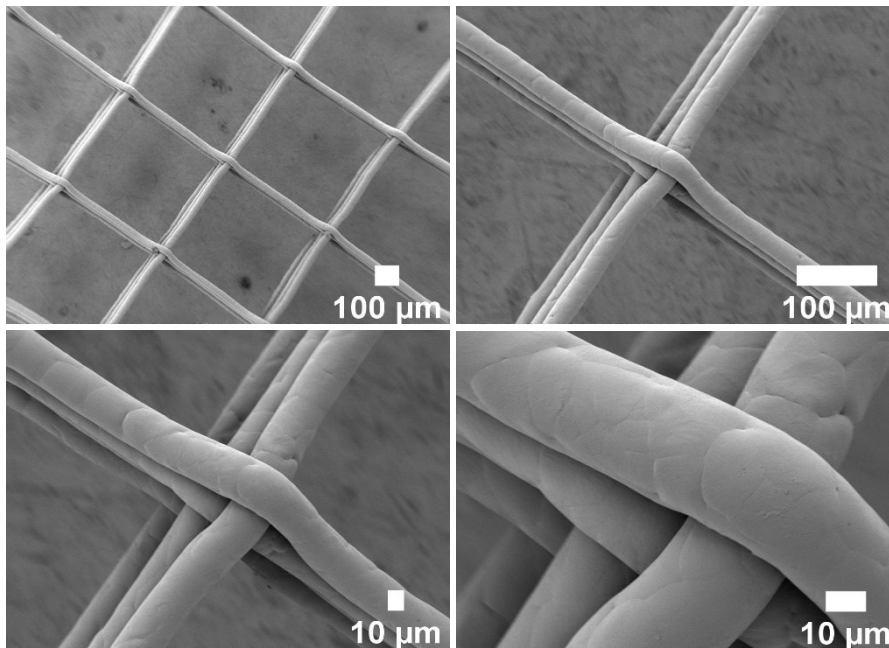


Figure 20. SEM images of the final PCL (Gesim) scaffold at (a) 150X, (b) 500X, (c) 1.00k X, (d) 2.50k X.

3.1.2 Optimization parameters of PCL (Sigma – Aldrich)

After the optimization of the PCL from the printer, the material was changed with PCL (Sigma – Aldrich), but using the parameters previously found, the fibers were no longer aligned and straight (*Fig. 21*).

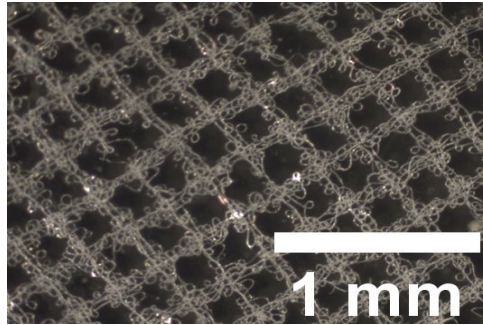


Figure 21. Microscope image 2X of PCL (Sigma – Aldrich) scaffold with parameters from PCL (Gesim).

Moreover, with the stand height of 0.250 mm, it was not possible to obtain all the predefined layers. It was therefore decided to lower it to 0.100 mm. Then, it was decided to decrease the infill distance from 0.450 mm to 0.300 mm, because it was seen from the literature [49] that a shorter infill distance allowed for more aligned fibers. When the infill distance was large, the electrostatic force attracted the material on the collector and not on the previously deposited fiber, whereas, when the infill distance was smaller, the incoming fibers are attracted by the previously deposited fiber.

So further tests were carried out to find the optimal parameters for this PCL.

Even though in literature [17-18, 20, 44-48] it was reported that the optimal pressure was at most 200 kPa, in this project there were no good results with lower pressure, so it was thought to increase the pressure and different tests were done at pressures of 200, 220, 240, 260 and 270 kPa, with the following constant parameters: temperature 85°C, voltage 4 kV, speed 25 mm/s, distance 1 mm, and 8 layers, finding 260 kPa to be the best. Then, other tests were done, changing the temperature from 75, 80, 85 to 90 °C, and the best result was 85°C. In particular, with a temperature of 70 and 75 °C the samples were too delicate and were damaged when removing them from the plate. Afterward, the voltage was tested (3, 3.5, 4, 4.5, 5 kV) and with 3 and 3.5 kV no results were obtained because the voltage was too low and the material was not extruded; whereas 4 kV was the better one, although in the literature the best voltage was supposed to be higher than 4.5 kV [17-18, 20, 44-48]. Therefore, speed was also tested. With a higher speed, it was possible to obtain more aligned and straighter fibers [19], so tests were done at the speed of 20, 25, 27 and 28 mm/s and the last one gave the best result. It was not possible to use a higher speed with this MEW printer. Then, with these new parameters, other tests were done changing the pressure (245, 250, 255, 260 kPa) and a better result was obtained with 255 kPa. Finally, it was analyzed the distance between the nozzle and the collector. It was tried with a distance higher than 2 mm, as suggested from the literature [17-18, 20, 44-48], but having a low voltage, the material was not extruded, so the tests were done with a distance lower than 1 mm (1 mm, 0.5 mm, 0.4 mm, 0.35 mm, and 0.3 mm). The best distance was 0.35 mm (*Fig. 22*).

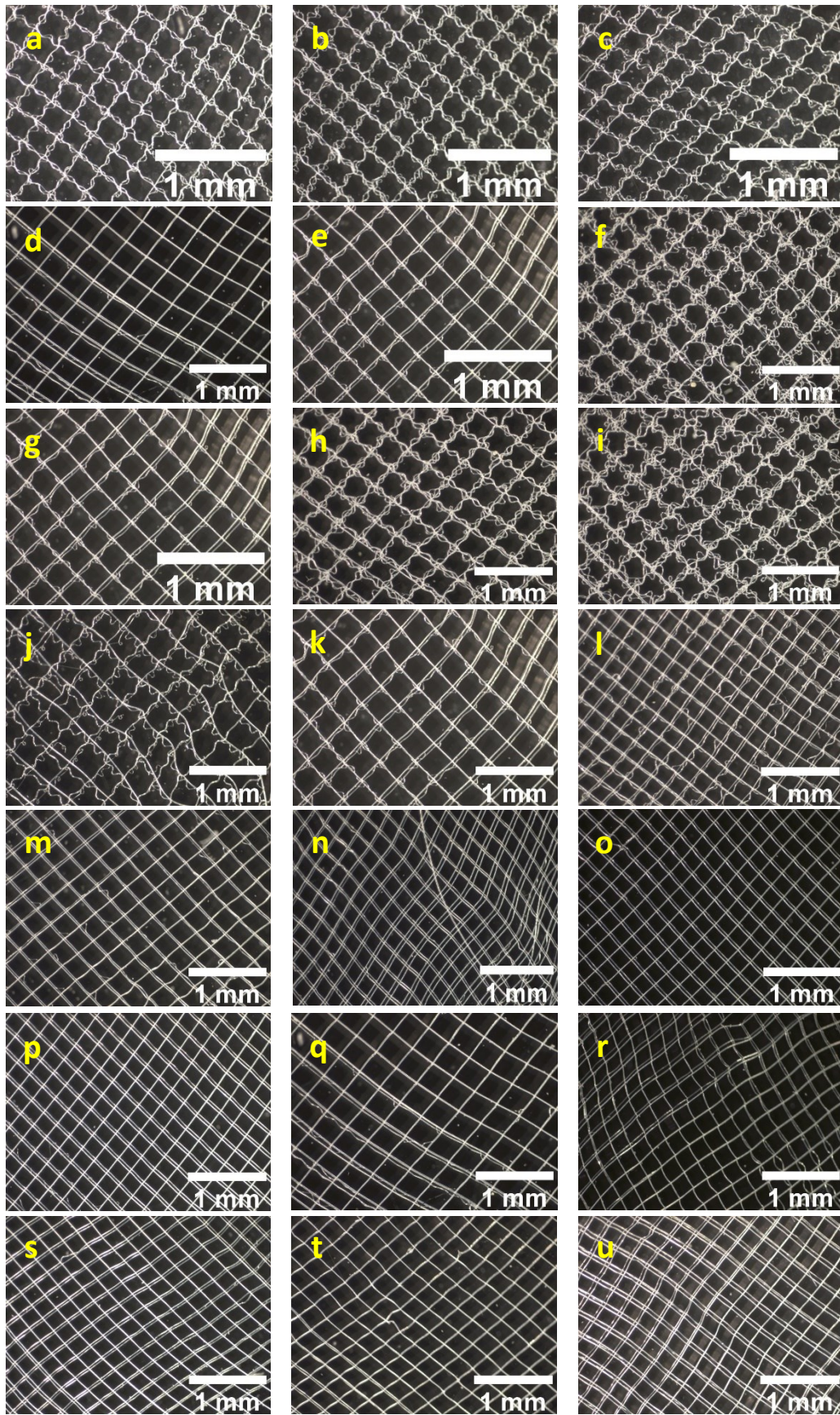


Figure 22. Microscope images 2X of (a) 200 kPa, (b) 220 kPa, (c) 240 kPa, (d) 260 kPa, (e) 85 °C, (f) 90 °C, (g) 4 kV, (h) 4.5 kV, (i) 5 kV, (j) 20 mm/s, (k) 25 mm/s, (l) 27 mm/s, (m) 28 mm/s, (n) 245 kPa, (o) 250 kPa, (p) 255 kPa, (q) 1 mm, (r) 0.5 mm, (s) 0.4 mm, (t) 0.35 mm (the best one), (u) 0.3 mm.

Thus, the optimal parameters to print PCL (Sigma Aldrich) scaffolds, in order to have straight and aligned fibers, were temperature of 85°C, pressure of 255 kPa, distance between collector and nozzle of 0.350 mm, speed of the cartridge 28 mm/s, voltage 4 kV, infill distance 0.325 mm, stand height 0.100 mm, 12 layers (*Fig. 23*). Fiber diameter and pore size of the final scaffold were measured by the software ImageJ. The fiber diameter was $31 \pm 3 \mu\text{m}$, while the pore size was $283 \pm 12 \mu\text{m}$ (x-axis) and $274 \pm 10 \mu\text{m}$ (y-axis). As can be seen (*Table 2*) there is a decrease in fiber diameter and pore size compared to the other from PCL (Gesim).

Table 2.

Material	Fiber diameter [μm]	x - Axis [μm]	y - Axis [μm]
PCL (Gesim)	44 ± 1	446 ± 8	450 ± 3
PCL (Sigma - Aldrich)	31 ± 3	283 ± 12	274 ± 10

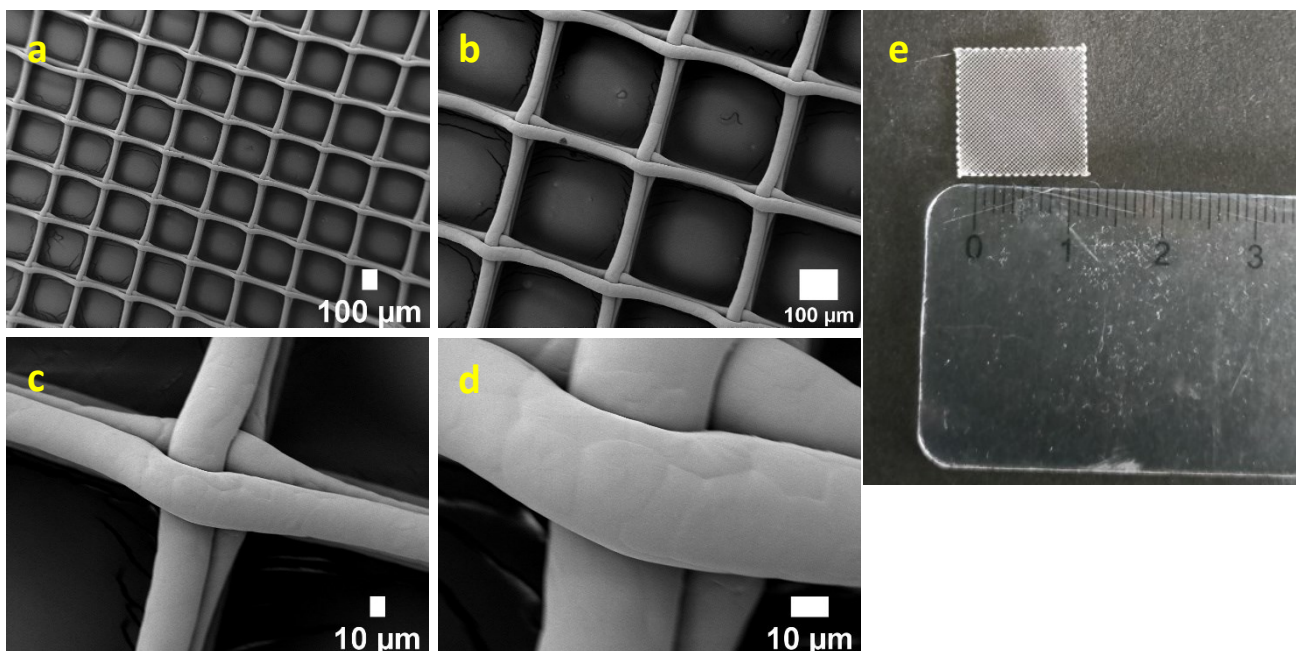


Figure 23. SEM images of the final PCL scaffold at (a) 100X, (b) 250X, (c) 1.00k X, (d) 2.50k X and (e) picture of the scaffold and a ruler to understand the size.

All the following analyses were carried out only in PCL (Sigma – Aldrich) samples.

3.1.3 Temperature measurement

As can be seen from *figure 24* the real temperature in the middle of the cartridge was similar at the different time points with an average value of $64.8 \pm 0.2 \text{ }^\circ\text{C}$. The same was for the tip of the cartridge with a mean temperature of $71.4 \pm 0.9 \text{ }^\circ\text{C}$. Thus, it was a good temperature to print PCL, because it was higher than its melting point ($60 \text{ }^\circ\text{C}$), but it was lower than $85 \text{ }^\circ\text{C}$, the temperature set on the code.

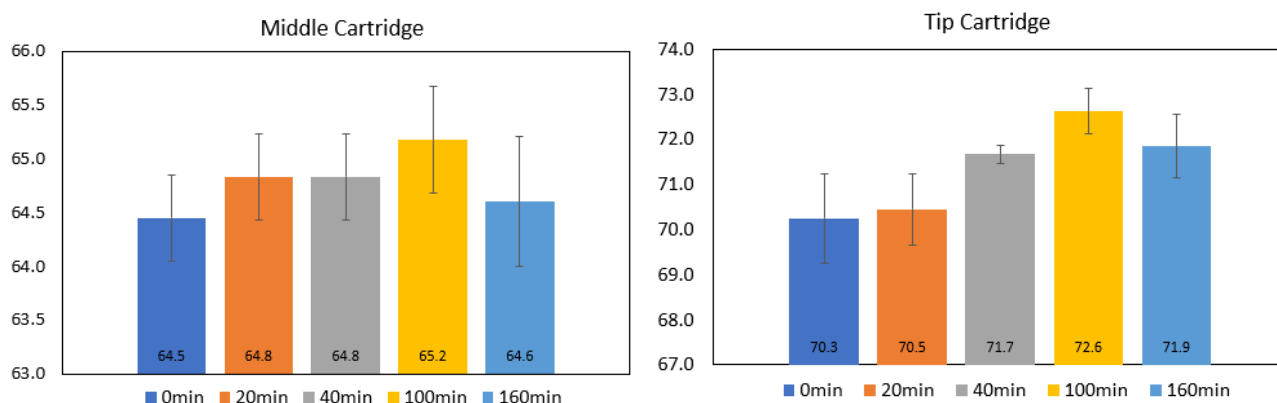


Figure 24. On the left, the average temperature of the middle of the cartridge at different time points. On the right, the average temperature of the tip of the cartridge at different time points.

3.2 Surface modification with alkaline hydrolysis treatment

After the alkaline hydrolysis treatment, fiber diameter and pore size were measured again, because it was supposed degradation of the fibers after the surface modification (Fig. 25). The diameter of the fibers decreased slightly following alkaline hydrolysis treatment, while the pore size did not change significantly. As can be seen in the SEM images (Fig. 26), there was a degradation of the surface of the fiber after 3 h of treatment.

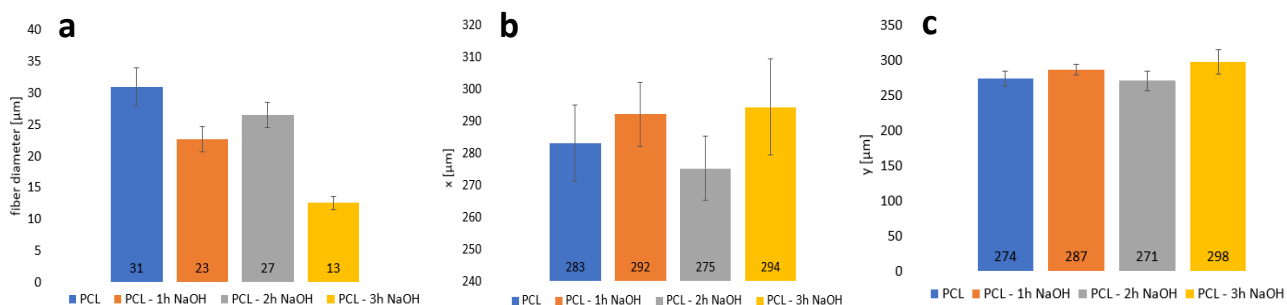


Figure 25. (a) Fiber diameter measure of pure PCL and PCL after 1 h, 2 h, 3 h of alkaline treatment. (b, c) Porus size of pure PCL and PCL after 1 h, 2 h, 3 h of alkaline treatment.

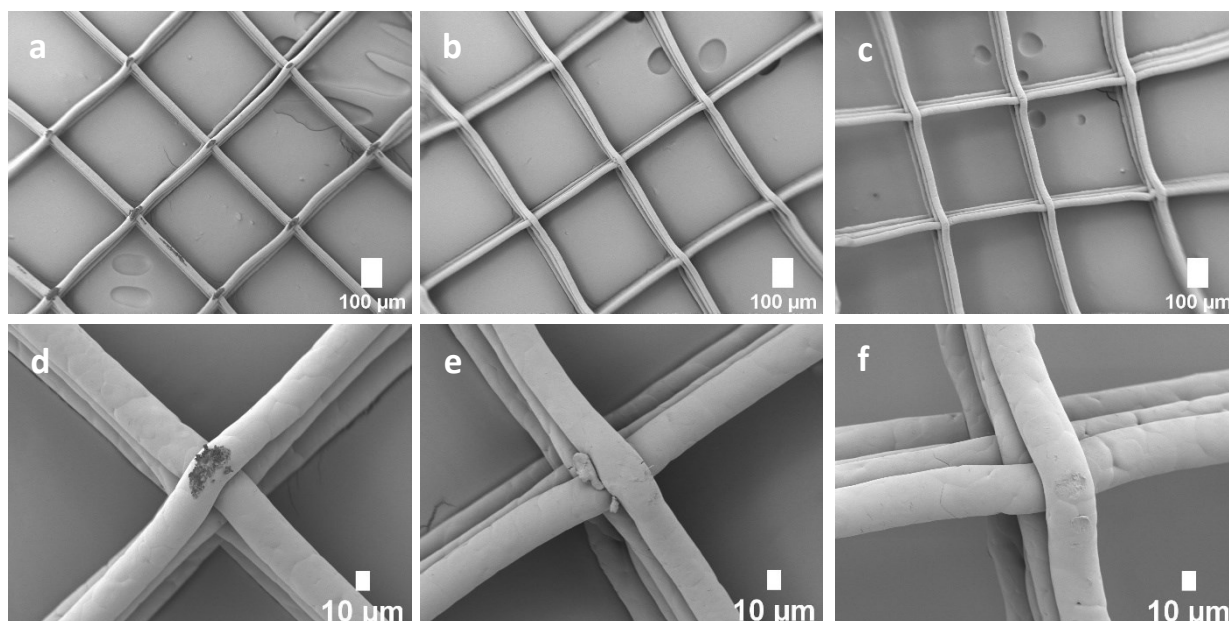


Figure 26. SEM images of PCL – 1 h NaOH (a) 150X and (d) 1.00k X, PCL – 2 h NaOH (b) 150X and (e) 1.00k X, PCL – 3 h NaOH (c) 150X and (f) 1.00k X.

The first analysis carried out to determine whether the treatment was successful was the FTIR analysis. As can be seen from *figure 27*, there are no differences between the surface chemistry of pure PCL scaffold and PCL with alkaline hydrolysis treatment scaffolds. The principal peaks of PCL, asymmetric and symmetric stretching of CH₂ bonds, respectively at 2945 – 2866 cm⁻¹, carbonyl stretching 1720 cm⁻¹, and asymmetric and symmetric stretching of C–O–C bonds, respectively at 1240 – 1168 cm⁻¹ [50], are similar in all the graphs.

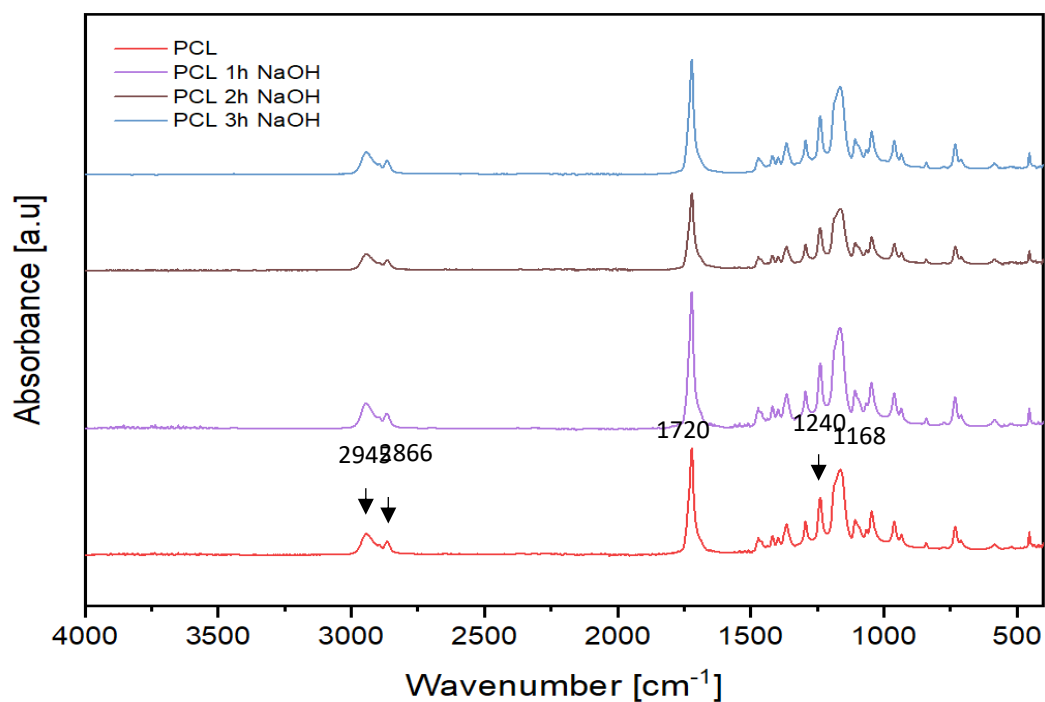


Figure 27. FTIR analysis of pure PCL, PCL – 1 h NaOH, PCL – 2 h NaOH, PCL – 3 h NaOH.

Since the surface chemistry analysis did not reveal the surface modification, it was decided to analyze the wettability of the scaffolds, because PCL is hydrophobic [50], but with this surface modification, it was supposed to become more hydrophilic [27, 51]. There was not so much difference between the contact angle of PCL scaffold (102 ± 2), PCL – 1 h NaOH (94 ± 4) and PCL – 2 h NaOH (100 ± 2) scaffold, but PCL – 3 h NaOH had a lower contact angle (85 ± 3), demonstrating that the surface was more hydrophilic than pure PCL, and therefore a likely success of the surface modification (Fig. 28).

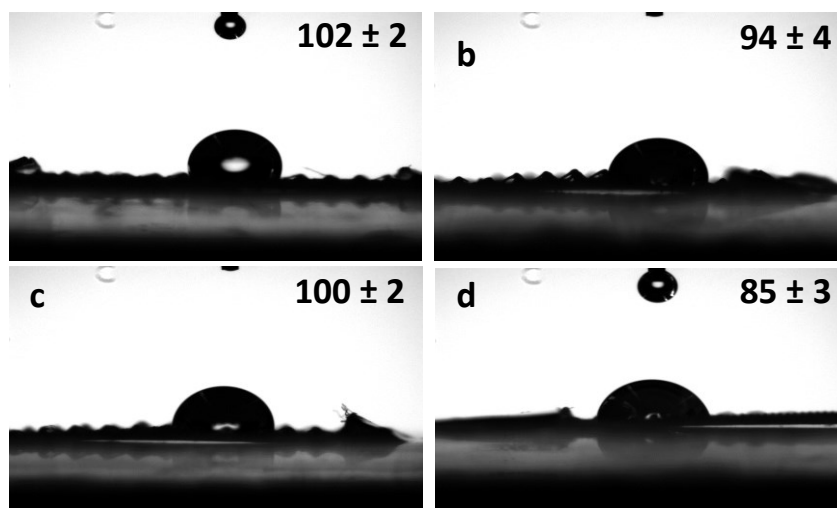


Figure 28. Contact angle of (a) PCL, (b) PCL – 1h NaOH, (c) PCL – 2 h NaOH, (d) PCL – 3 h NaOH.

Finally, also the antioxidant activity was analyzed to determine the success of the alkaline hydrolysis treatment. After the treatment, in all cases, there was an increase in DPPH radical scavenging activity, from 4% for pure PCL to a mean of 11% for the treated scaffolds. It can be seen that the solution, containing the scaffold with 3 h of treatment, changed color, as proof of antioxidant activity and of the surface treatment carried out (Fig. 29).

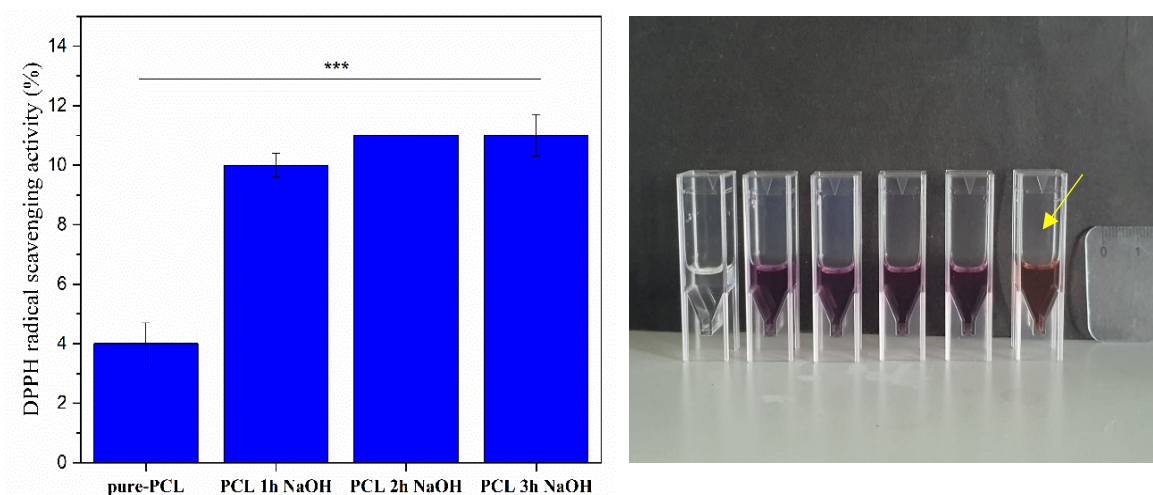


Figure 29. On the left, the antioxidant graph. On the right, in order, from the left: Methanol, cnt, PCL, PCL – 1h NaOH, PCL – 2h NaOH, PCL – 3h NaOH.

3.3 Magnetic Nanoparticles morphology

The morphology of nanoparticles was analyzed in previous work [13]. Transmission Electron Microscopy (TEM) analysis evidenced the pseudo-spherical shape of both MNPs and Si-MNPs and measured diameter of 10-15 nm. Moreover, a silica coating of 1-2 nm was present around the magnetic core of Si-MNPs (*Fig. 30*).

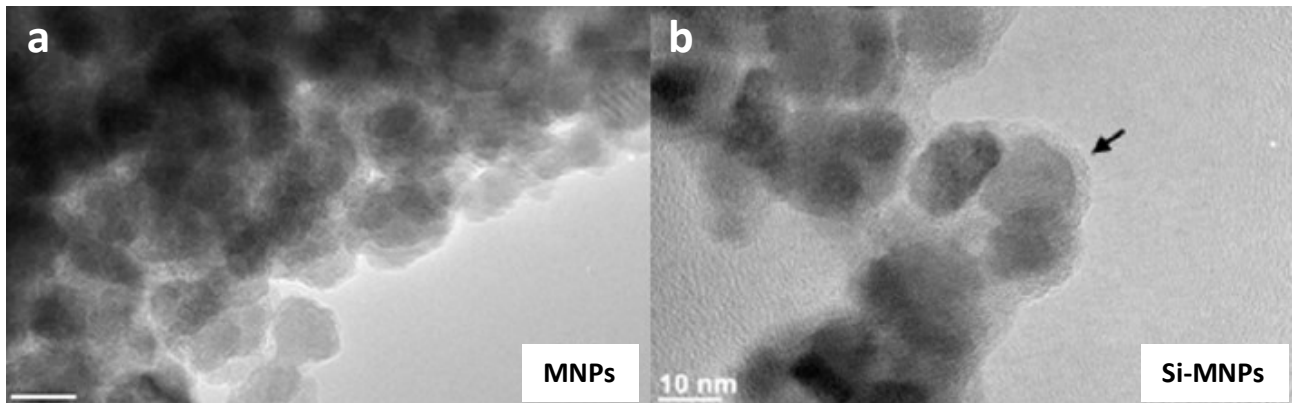


Figure 30. TEM images of a) MNPs and b) Si-MNPs.

3.4 PCL melt electrowritten scaffolds with MNPs and Si-MNPs coating

After the surface modification with the alkaline treatment, the coating with MNPs or Si-MNPs was carried out (*Fig. 31*, *Fig. 32*).

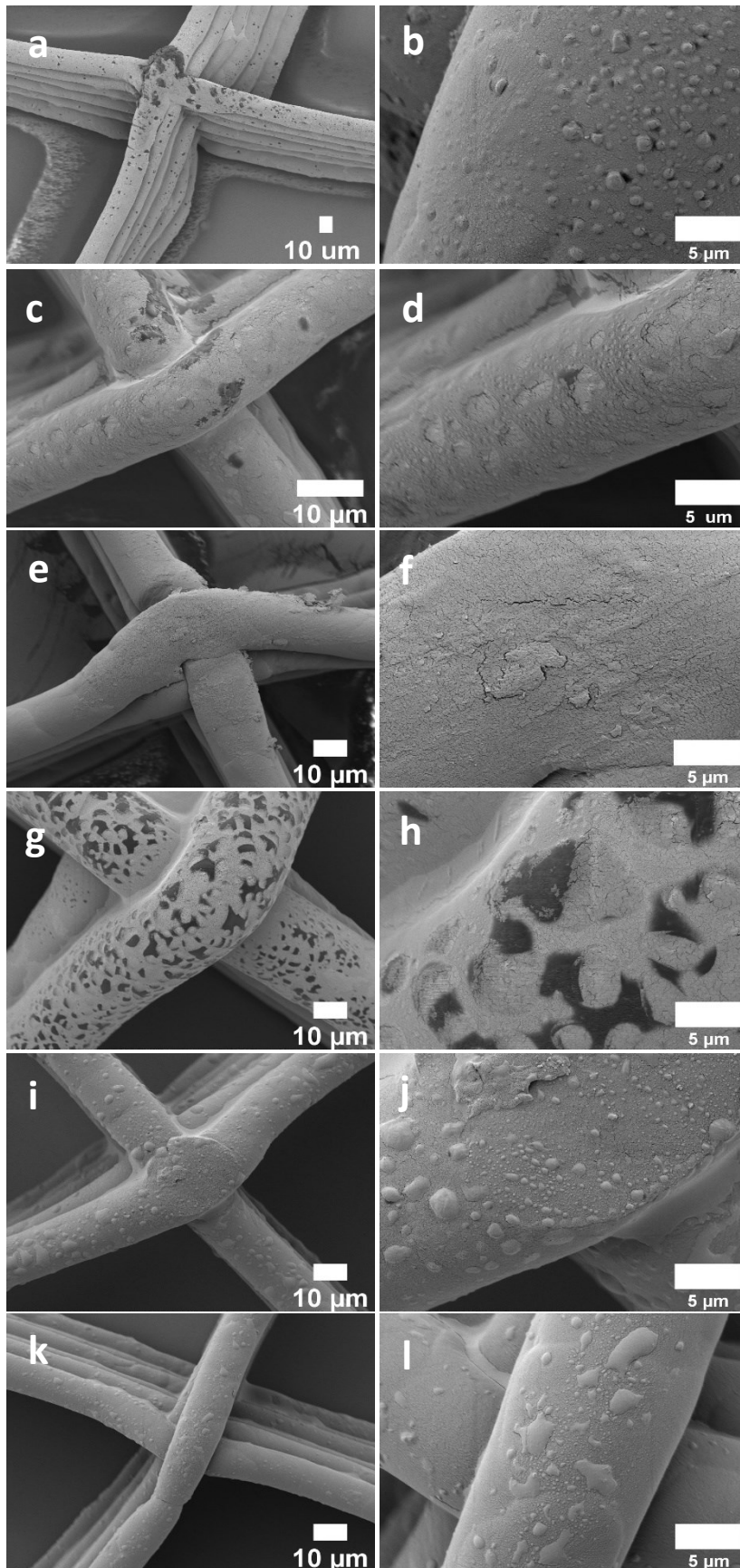


Figure 31. SEM images at different magnification of (a, b) PCL – 1 h NaOH – 1 min MNPs, (c, d) PCL – 1 h NaOH – 3 min MNPs, (e, f) PCL – 2 h NaOH – 1 min MNPs, (g, h) PCL – 2 h NaOH – 3 min MNPs, (i, j) PCL – 3 h NaOH – 1 min MNPs, (k, l) PCL – 3 h NaOH – 3 min MNPs.

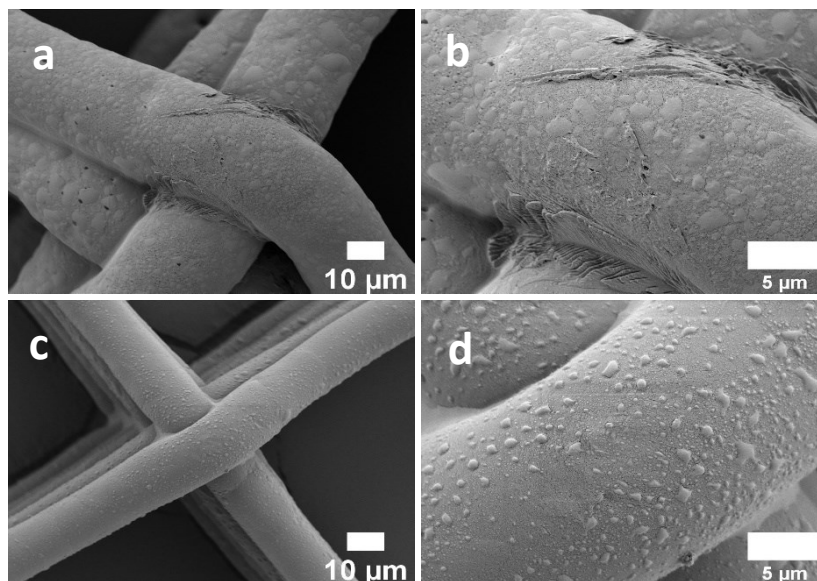


Figure 32. SEM images a different magnification of (a, b) PCL – 3 h NaOH – 1 min Si-MNPs, (c, d) PCL – 3 h NaOH – 3 min Si-MNPs.

Since the three-hour alkaline treatment was the most efficient, it was ultimately decided to analyze only samples with three hours of treatment for subsequent studies.

FTIR analysis was performed to detect variations in the peaks that would demonstrate the presence of the nanoparticle coating. The FTIR spectra (Fig. 33) showed a decrease in the typical PCL peaks and also an increase in 580 cm^{-1} peak, as well as the presence of the peak at 631 cm^{-1} , typical Fe – O bond vibration peaks [52-53], which demonstrated the presence of MNPs on the surface of the samples. Moreover, for samples containing Si-MNPs, there was an appearance of absorption band at 800 cm^{-1} , attributed to the symmetric stretching band of -Si-O-Si- [54].

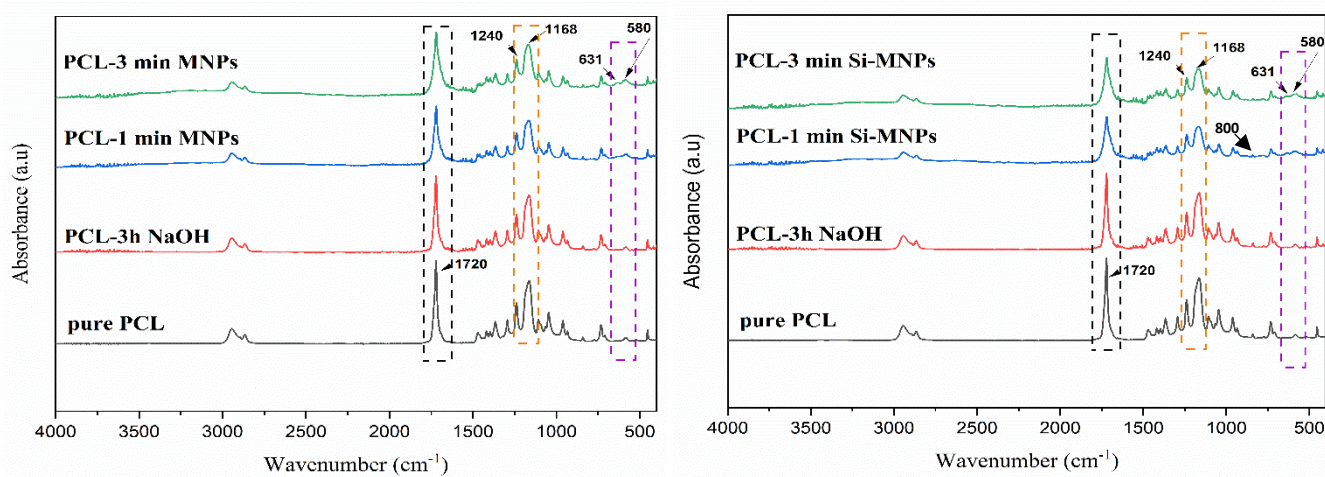


Figure 33. FTIR analysis of PCL scaffold with: on the left MNPs coating, on the right Si-MNPs coating.

3.5 Release of MNPs and Si-MNPs in medium

The stability of MNPs and Si-MNPs coating on the PCL scaffold with alkaline hydrolysis treatment was analyzed by ATR-FTIR analysis, SEM images, and the measure of the pH medium to assess a possible release of nanoparticles.

As could be seen in *figure 34*, for each kind of scaffold, there was a slight increase in the medium pH after 7 days compared to 1 day of incubation which may represent a probable release of ions, but further investigations should be carried out.

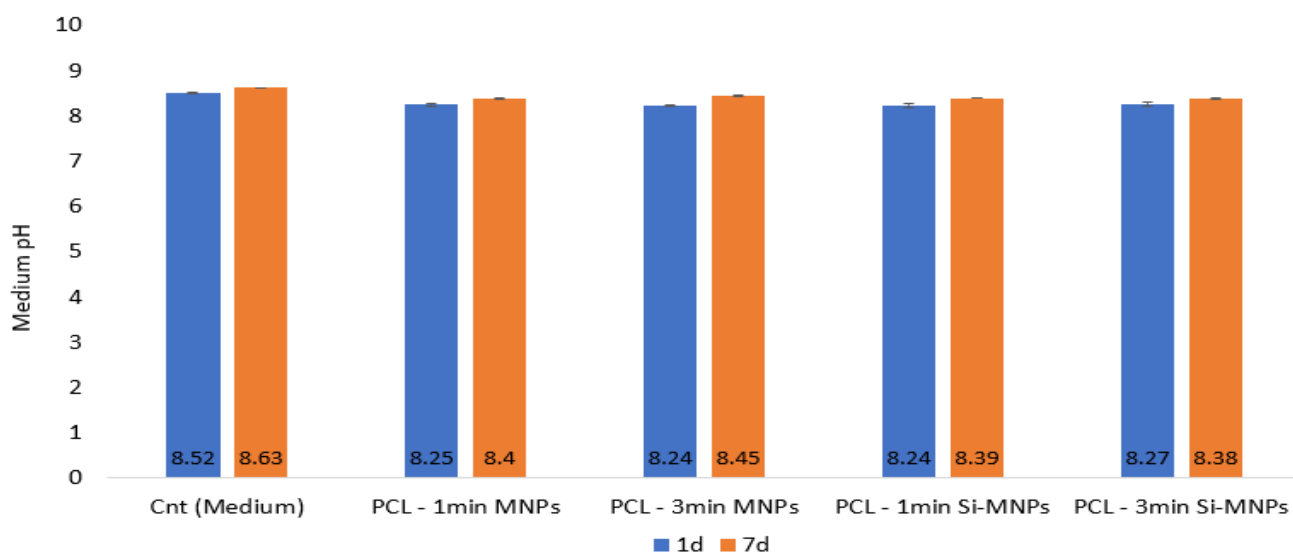


Figure 34. pH measurement after 1 day and after 7 days of incubation of samples.

The stability of the NPs was studied also with FTIR analysis (*Fig. 35*) where there was an increase in the carbonyl stretching peak (1720 cm^{-1}) and in the asymmetric and symmetric stretching of C–O–C bond peaks ($1240 - 1168\text{ cm}^{-1}$), for every type of scaffold, with MNPs and with Si-MNPs. Moreover, the 580 cm^{-1} Fe – O bond vibration peak disappeared after 7 days in medium, which demonstrated a possible release of nanoparticles.

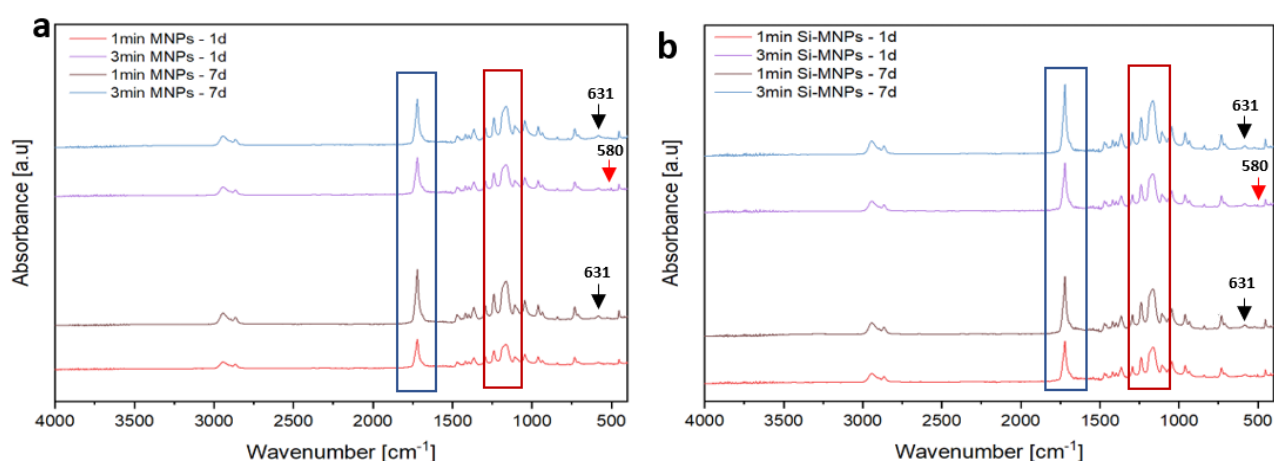


Figure 35. (a) FTIR analysis of PCL – 1 min MNPs and PCL – 3 min MNPs after 1 day and 7 days. (b) FTIR analysis of PCL – 1 min Si-MNPs and PCL – 3 min Si-MNPs after 1 day and 7 days.

Since from the analysis the coating seemed to be more efficient after 3 min, it was decided to continue analyzing the samples with 3 min of MNPs and Si-MNPs coating.

3.6 Mechanical strength test

The tensile strength of the samples with different modifications (PCL – 3 h NaOH, PCL – 3 min MNPs, PCL – 3 min Si-MNPs) was compared to that of pure PCL, to see if they had different mechanical behaviors. The stress–strain curve showed a decrease in both stress and strain in modified samples compared to pure PCL (*Fig. 36 a*). The Young’s Modulus did not change significantly (0.4 ± 0.1 MPa for the PCL scaffold, while 0.3 ± 0.1 MPa for the other samples), which means that the stiffness remained the same even after alkaline hydrolysis treatment and nanoparticle coating (*Fig. 36 b*). The elongation at the break had no relevant differences after the modifications (39 ± 4 % for PCL, 34 ± 4 % for PCL – 3 h NaOH, 24 ± 4 for PCL – 3 min MNPs, 25 ± 6 for PCL – 3 min Si-MNPs) (*Fig. 36 c*). The tensile strength decreased after the alkaline hydrolysis treatment, probably due to the degradation involved (12 ± 2 MPa for PCL, 7 ± 1 for PCL – 3 h NaOH, 5 ± 2 for PCL – 3 min MNPs, 6 ± 1 for PCL – 3 min Si-MNPs) (*Fig. 36 d*), thus further studies should be carried out to assess whether the mechanical behavior of these scaffolds in vivo is still acceptable.

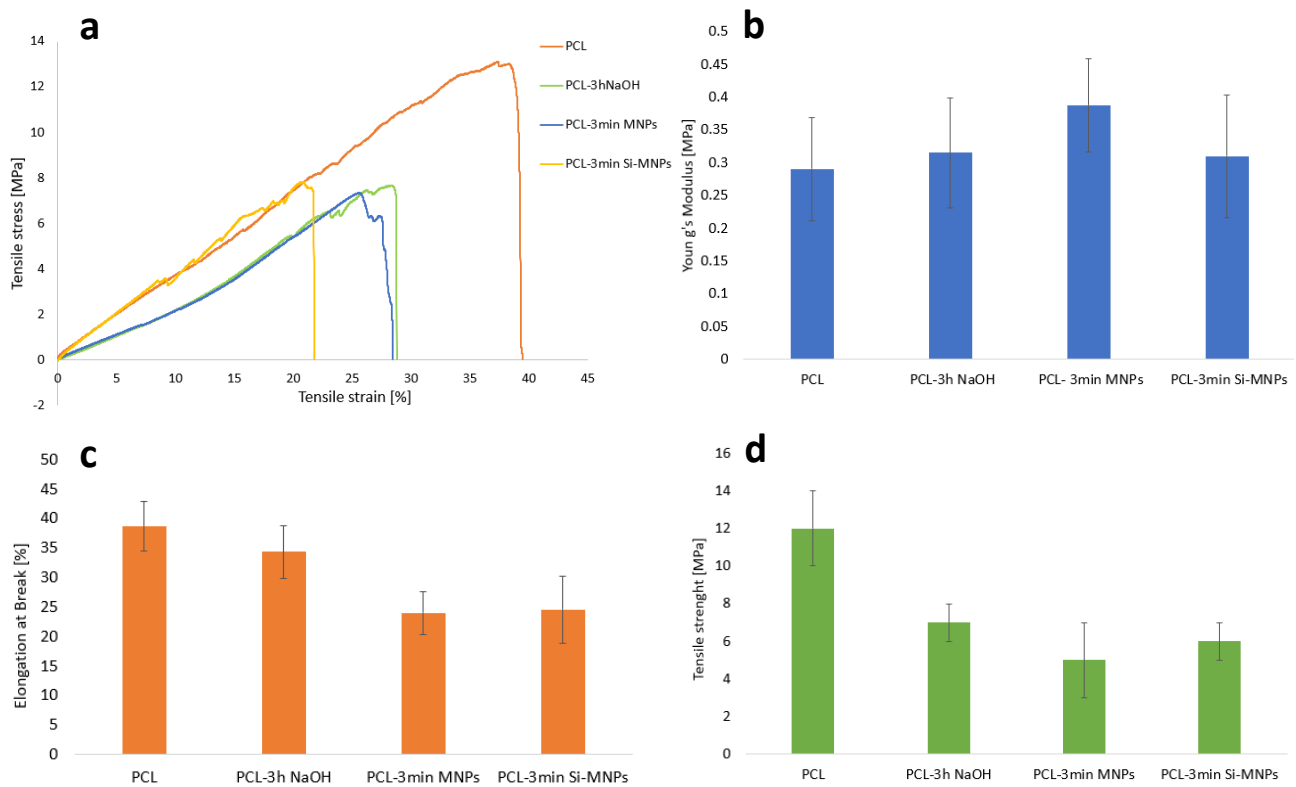


Figure 36. (a) Tensile stress-strain graph, (b) Young’s Modulus, (c) elongation at break, (d) tensile strength bar charts.

3.7 Antioxidant Activity

Antioxidants are interesting in biomedical applications because of protecting the cells from free radicals' oxidative damage [61]. In literature, some papers talk about an effective scavenging assay of MNPs [55-56], and it was seen that polymers functionalized with citric acid may have antioxidant properties [63-64], so it was chosen to analyze the antioxidant activity of these scaffolds, using DPPH method, after the coating with nanoparticles.

As can be seen (Fig. 37), even though the presence of iron oxides, in both MNPs and Si-MNPs coating, there was an increase in radical scavenging activity from 4% for pure PCL samples to 16% for samples with NPs coating, which demonstrated a slightly antioxidant activity. The antioxidant activity could therefore increase due to the presence of citric acid.

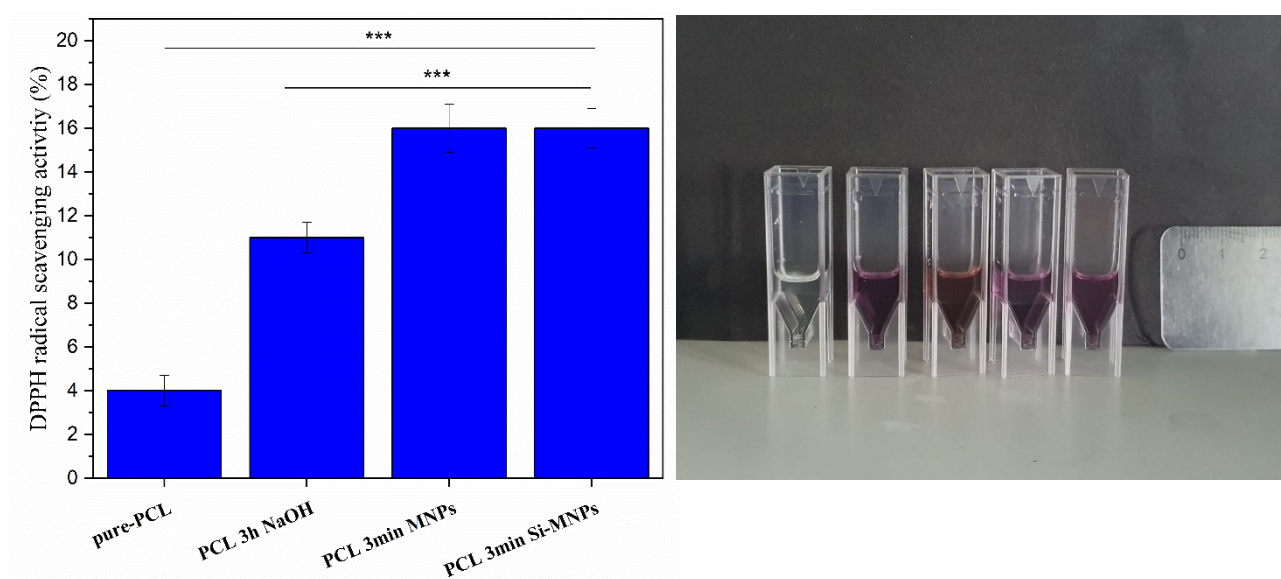


Figure 37. On the left, the antioxidant graph. On the right, in order, from the left: Methanol, cnt, PCL, PCL – 3h NaOH, PCL – 3 min MNPs, PCL – 3 min Si-MNPs.

3.8 Antibacterial Activity

MNPs could have antibacterial activity [39, 41], and bactericidal activity for the reactive oxygen species (ROS) that they produce. ROS produced hydrogen peroxide which could enter the cell membrane of bacteria and kill them [42, 56]. Moreover, this study [40] showed that Si-MNPs could trap bacteria and inhibit their biofilm formation.

Here, the antibacterial activity of the samples was analyzed with *S. aureus* (Gram-positive) and *E.coli* (Gram-negative) bacteria. As can be seen (Fig. 38), the incorporation of the nanoparticles produced a slightly antibacterial effect for both *S. aureus* and *E.coli* bacteria strains at 6 h.

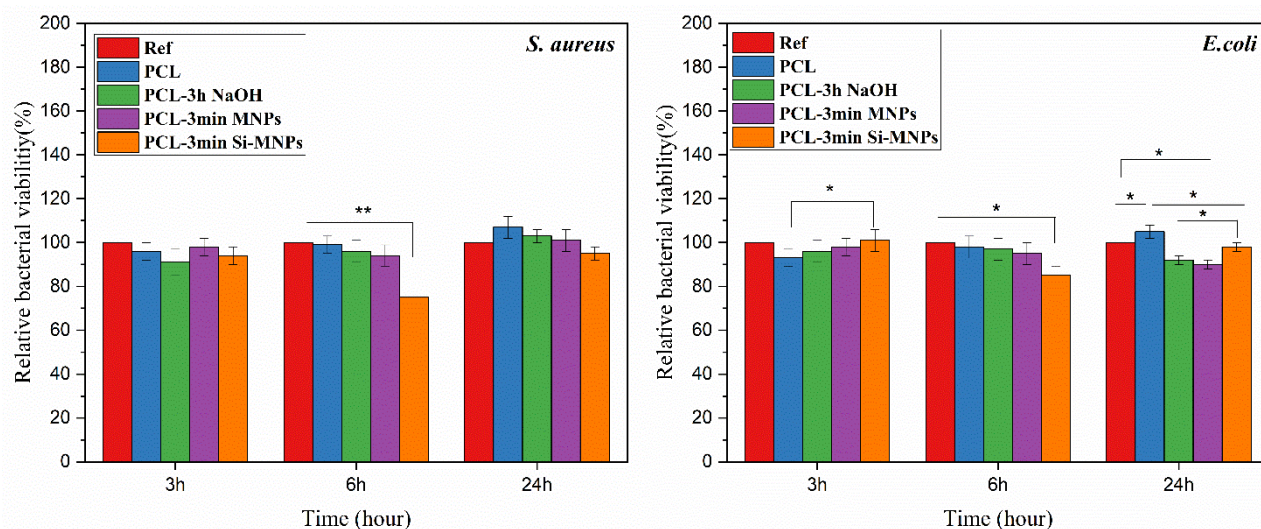


Figure 38. Antibacterial activity of PCL, PCL – 3 h NaOH, PCL – 3 min MNPs, PCL – 3 min Si-MNPs scaffolds after 3, 6, and 24 h incubation with *S. aureus* (Gram-positive) on the left, and *E. coli* (Gram-negative) bacteria on the right.

3.9 Biological Activity

3.9.1 Cytotoxicity analysis – Indirect Study with MG-63 osteoblast-like cells

The indirect contact test with MG-63 cells was used to analyze the cytotoxicity of PCL, PCL – 3 h NaOH, PCL – 3 min MNPs, PCL – 3 min Si-MNPs scaffolds. The measurements were carried out by WST-8 cell proliferation assay. The viability of MG-63 cells increased by over 50% compared to the control (culture without scaffold) after 48 h of incubation with the samples, proving that scaffolds and in particular MNPs and Si-MNPs were not cytotoxic and cell compatible (Fig. 39), as previously demonstrated by other studies involving different MNPs-containing scaffolds [47, 57].

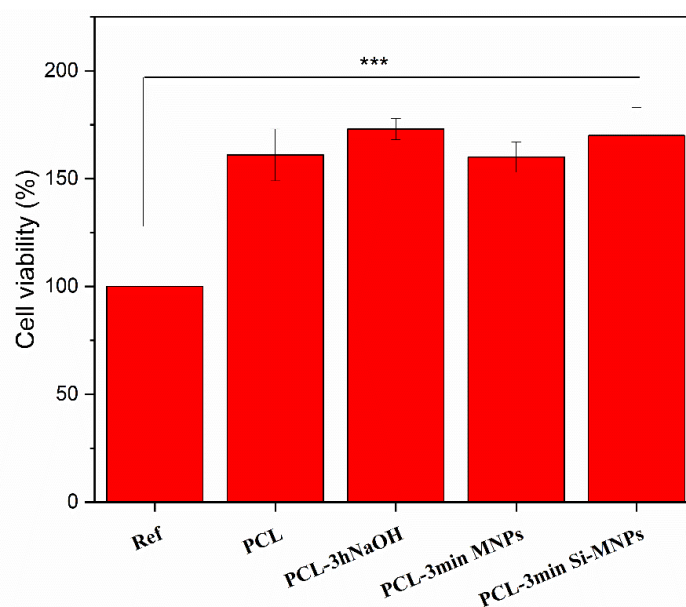


Figure 39. MG-63 cell viability graph of cells (Ref), PCL, PCL – 3 h NaOH, PCL – 3 min MNPs, PCL – 3 min Si-MNPs.

It can be observed from fluorescence images (*Fig. 40*) that cells were present in the scaffolds. In fact, in both DAPI – Calcein and DAPI – Phalloidin images, nuclei and cytoplasm, and nuclei and actin filament, respectively, were present. The fluorescence images were in agreement with the cell viability analyzed before.

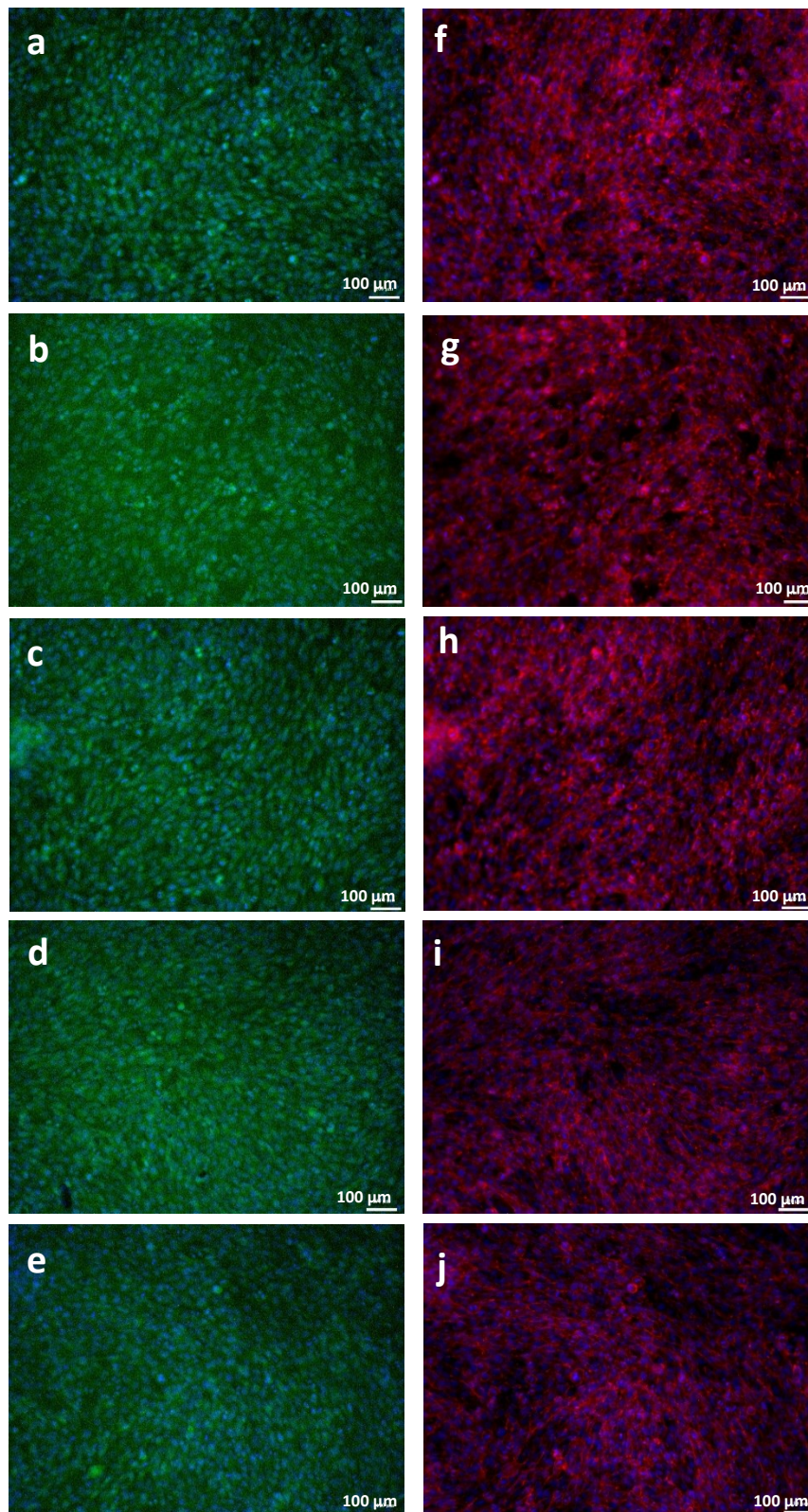


Figure 40. Fluorescence images: on the left, DAPI (nuclei) and phalloidin (cytoplasm) of (a) control (MG63), (b) PCL, (c) PCL – 3h NaOH, (d) PCL – 3min MNPs, (e) PCL – 3min Si-MNPs. On the right, DAPI (nuclei) and phalloidin (F-actin) of (f) control (MG63), (g) PCL, (h) PCL – 3h NaOH, (i) PCL – 3min MNPs, (j) PCL – 3min Si-MNPs.

3.9.2 Cell proliferation analysis - Direct study with MC3T3-E1 pre-osteoblast cells

To study cell proliferation on samples, a direct contact method was used, and the measurements were carried out by WST-8 cell proliferation assay. The viability of MC3T3-E1 cells increased from more than 100% after 1 day of incubation (except for PCL - 3 min Si-MNPs where initially the viability was lower than the control) to almost 500% for PCL - 3 min MNPs and to more than 600% for PCL - 3 min Si-MNPs after 7 days of incubation with the samples compared to the control (PCL scaffold), proving that scaffolds with NPs coating are cell compatible, as well as a good environment for cell proliferation (Fig. 41).

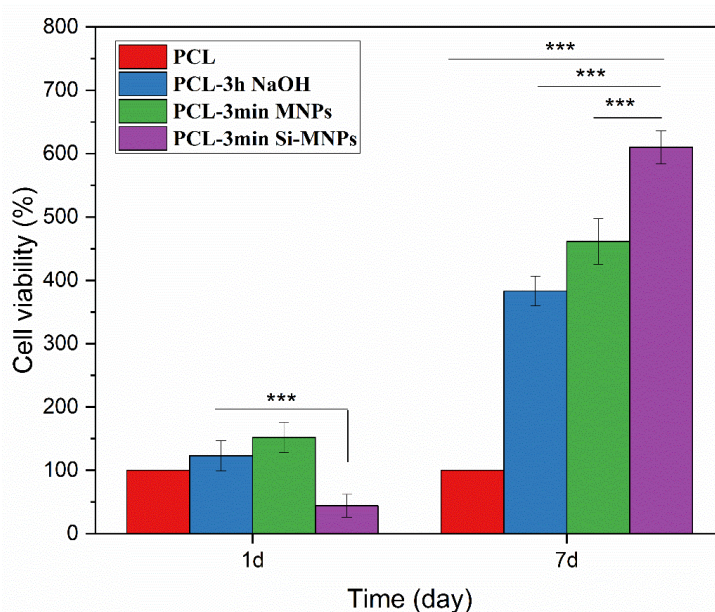


Figure 41. MC3T3-E1 cell viability graph of PCL (control), PCL - 3 h NaOH, PCL - 3 min MNPs, PCL - 3 min Si-MNPs after 1 day (on the left) and after 7 days (on the right).

The fluorescence images (Fig. 42, Fig. 43) showed the cell proliferation on the scaffolds (PCL, PCL - 3 h NaOH, PCL - 3 min MNPs, PCL - 3 min Si-MNPs) after 1 day and after 7 days. It can be seen that only PCL scaffold (Fig. 42 a, e, Fig. 43 a, e) had no good cell proliferation either after 7 days. PCL - 3 h NaOH (Fig. 42 b, f, Fig. 43 b, f) had a huge cell proliferation after 7 days, but the cells were not attached to the scaffold. For PCL - 3 min MNPs (Fig. 42 c, g, Fig. 43 c, g) and more for PCL - 3 min Si-MNPs (Fig. 42 d, h Fig. 43 d, h), after 7 days, cells proliferated and were attached to the fibers, proving that the nanoparticles improved cells adhesion and proliferation, as was reported in literature [58-60]. In several studies, the MNPs' behavior with cells has been analyzed. For example, in one paper it was reported that the presence of MNPs in ceramic scaffolds increased cell proliferation [58]. Moreover, the presence of MNPs in PCL scaffolds improved cell adhesion due to the higher hydrophilicity of the surface of the scaffold, and consequently also increased cell proliferation [59]. Finally, in another study, the result was an increase in cell growth and proliferation, when PCL scaffolds were functionalized with MNPs [60].

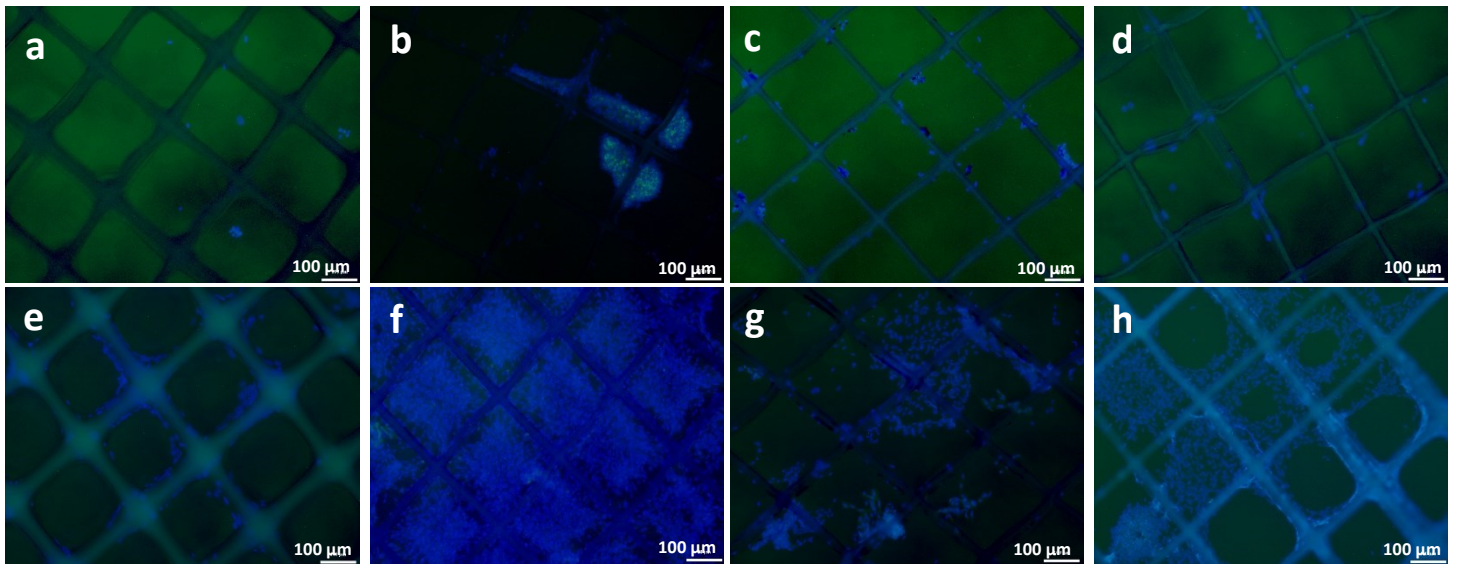


Figure 42. Fluorescence images: DAPI (nuclei) and calcein (cytoplasm) of (a) control (PCL) after 1 day and (e) after 7 days, (b) PCL – 3 h NaOH after 1 day and (f) after 7 days, (c) PCL – 3 min MNPs after 1 day and (g) after 7 days, (d) PCL – 3 min Si-MNPs after 1 day and (h) after 7 days.

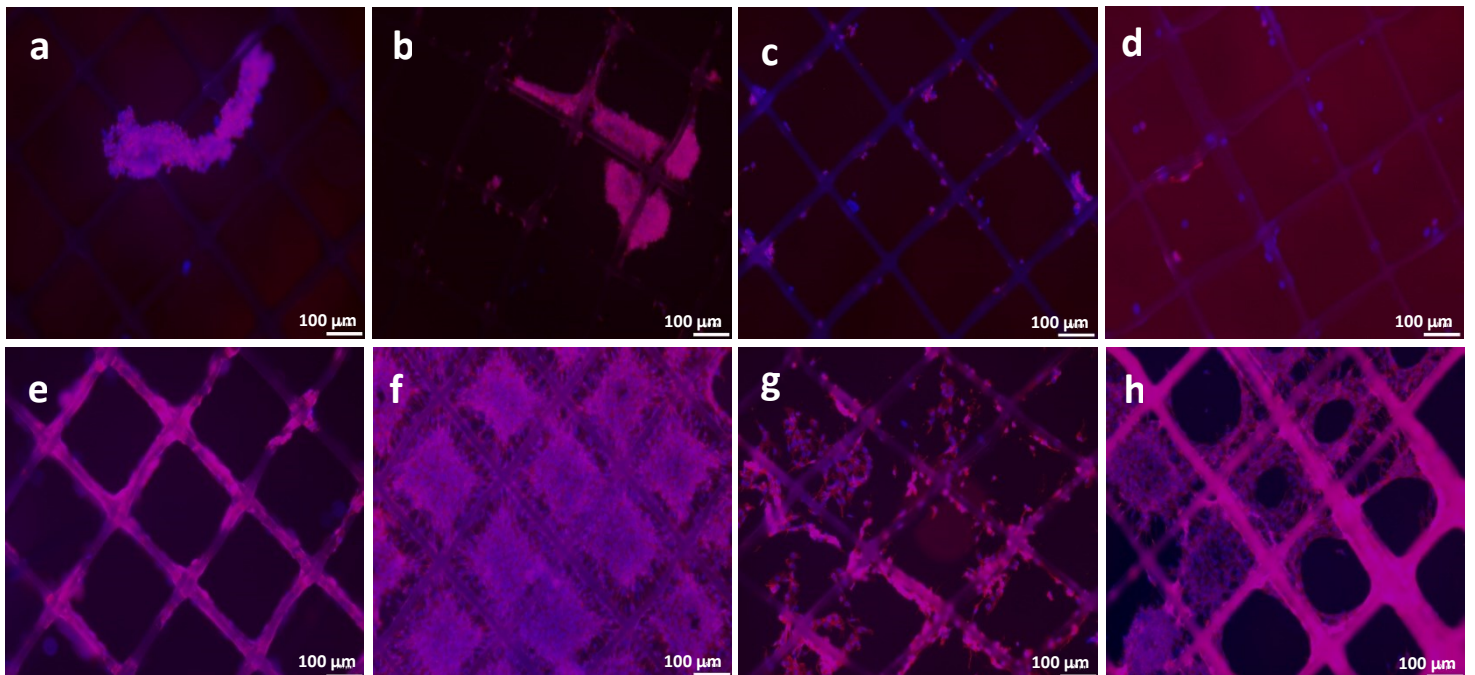


Figure 43. Fluorescence images: DAPI (nuclei) and phalloidin (f-actin) of (a) control (PCL) after 1 day and (e) after 7 days, (b) PCL – 3 h NaOH after 1 day and (f) after 7 days, (c) PCL – 3 min MNPs after 1 day and (g) after 7 days, (d) PCL – 3 min Si-MNPs after 1 day and (h) after 7 days.

4. Conclusion and future development

The current treatments for bone cancer are surgery, chemotherapy, and radiation therapy. Nevertheless, surgery often does not remove the whole tumor, which causes the appearance of metastases, and chemotherapy often does not solve the problem of metastases. The result is a high mortality rate for bone cancer and most of the patients die from lung metastases.

Thanks to the development of bionanotechnology, new advanced treatment opportunities for bone cancer therapy are researched and developed every day. In particular, these treatment methods are based on biomaterials and can decrease the side effects, by using a selective and local delivery. The main task of biomaterials for bone cancer therapy is to kill cancer cells and to help bone regeneration. For example, magnetic nanoparticles can be used in vivo for hyperthermia, which kills cancer cells through heat. Another example can be the use of biomaterials to realize scaffolds for bone tissue regeneration after surgery, to repair bone defects.

The present thesis was focused on the development of a PCL scaffold with magnetic nanoparticles coating, for bone cancer treatment. The work started in *Politecnico di Torino*, where magnetic nanoparticles (MNPs) and magnetic nanoparticles with silica-shell were synthesized (Si-MNPs) using the co-precipitation method.

Then, the rest of the experimental part of the thesis was carried out at *Friedrich-Alexander-Universität, Erlangen-Nürnberg*. PCL scaffolds were realized with the melt electrowriting (MEW) additive manufacturing method, then they were functionalized with alkaline hydrolysis treatment to improve the hydrophilicity of the surface and a coating with MNPs or Si-MNPs was carried out. After that, the chemical, physical and biological properties of the different kinds of scaffolds were analyzed.

At the beginning, PCL (Gesim) was used and the optimal parameters to print it with MEW were found, then it was changed because the MEW company didn't sell the material. Thus, PCL 45kDa (Sigma-Aldrich) was used and the optimal parameters were temperature of 85°C, pressure of 255 kPa, distance between collector and nozzle of 0.350 mm, speed of the cartridge 28 mm/s, voltage 4 kV, infill distance 0.325 mm, stand height 0.100 mm, 12 layers. The fiber diameter was $31 \pm 3 \mu\text{m}$, while the pore size was $283 \pm 12 \mu\text{m}$ (x-axis) and $274 \pm 10 \mu\text{m}$ (y-axis).

PCL is a perfect biomaterial for MEW method because it has a low melting point (60 °C) and it is biocompatible, biodegradable, with mechanical strength and low cost. The defect of PCL is that it is hydrophobic, not allowing good adhesion to particles and cells. For this reason, surface modification with alkaline treatment was carried out to improve the hydrophilicity of the scaffold. With more details, the scaffolds were immersed in the alkaline solution (NaOH + water) for 1 h, 2 h, or 3 h. After the treatment, the diameter of the fibers decreased slightly, due to the degradation induced by NaOH. Several analyses were carried out to understand if the treatment was successful. Through the FTIR analysis, there were no differences between the pure PCL band and the bands of PCL + alkaline treatment at three different time points. So, the wettability of the scaffolds was analyzed, and even though there was no relevant difference between the contact angles of PCL (102 ± 2), PCL - 1 h NaOH (94 ± 4), and PCL - 2 h NaOH (100 ± 2) samples, the contact angle of PCL - 3 h NaOH scaffold was lower (85 ± 3), proving that the surface was more hydrophilic than pure PCL. Moreover, antioxidant analysis with DPPH radical

scavenging activity was carried out always to prove the surface modification, and with the alkaline hydrolysis treatment, there was an increase of DPPH from 4% for PCL, to a mean of 11% for PCL with the treatment. Additionally, the solution, where PCL – 3 h NaOH samples were immersed, changed color as proof of antioxidant activity and of the surface treatment carried out. So, the best surface modification was that one with 3 h of alkaline treatment.

After the surface modification, the nanoparticles coating on the scaffolds was performed. The FTIR analysis was effectuated and there was a decrease in the mean peaks of PCL (asymmetric and symmetric stretching of CH₂ bonds, respectively 2945 – 2866 cm⁻¹, carbonyl stretching 1720 cm⁻¹, and asymmetric and symmetric stretching of C–O–C bonds, respectively 1240 – 1168 cm⁻¹) after the coating, as well as an increase in 580 cm⁻¹ peak, and the presence of the peak at 631 cm⁻¹, which are typical Fe – O bond vibration peaks. In Si-MNPs coating scaffolds, there was an appearance of absorption band at 800 cm⁻¹, attributed to the symmetric stretching band of -Si-O-Si-. These results demonstrate the presence of MNPs or Si-MNPs on the surface of the scaffolds.

The stability of the nanoparticles coating the scaffold was analyzed in medium after 1 day and after 7 days of incubation, measuring the medium pH that increased slightly after 7 days; and with FTIR analysis, that showed an increase in the carbonyl stretching peak (1720 cm⁻¹) and in the asymmetric and symmetric stretching of C–O–C bonds peaks (1240 – 1168 cm⁻¹), for every type of scaffold, with MNPs and with Si-MNPs. Moreover, the 580 cm⁻¹ Fe – O bond vibration peak disappeared after 7 days in medium, which demonstrated a possible release of nanoparticles.

Then, the tensile strength of the samples with different modifications (PCL – 3 h NaOH, PCL – 3 min MNPs, PCL – 3 min Si-MNPs) was compared to that of pure PCL, to see if they had different mechanical behaviors. The stress–strain curve showed a decrease in both stress and strain in modified samples compared to pure PCL. The Young's Modulus did not change significantly, which means that the stiffness remained the same even after alkaline hydrolysis treatment and nanoparticle coating. The elongation at the break had no relevant differences after the modifications and the tensile strength decreased slightly after the treatment and the nanoparticle coating. Overall, the material retained good magnetic properties even after alkaline treatment and nanoparticle coating.

Afterwards, the antioxidant activity of the coated scaffolds was studied. There was a further increase in the radical scavenging activity to 16% for samples with NPs coating, which demonstrated antioxidant activity of both MNPs and Si-MNPs.

The antibacterial activity was carried out by analyzing the scaffolds' behavior with *S. aureus* and *E. coli*. In both studied cases, the incorporation of the nanoparticles produced a slightly antibacterial effect for both *S. aureus* and *E. coli* bacteria strains at 6 h.

Finally, the biological activity was studied through an indirect contact test to study the cytotoxicity and a direct method to study the cell proliferations.

The cytotoxicity was analyzed with MG-63 cells incubated for 48 h with PCL, PCL – 3 h NaOH, PCL – 3 min MNPs, PCL – 3 min Si-MNPs scaffolds. The viability of MG-63 cells increased by over 50% compared to the control, proving that scaffolds and in particular MNPs and Si-MNPs were not cytotoxic and cell compatible.

The cell proliferation was studied by analyzing the viability of MC3T3-E1 cells on the scaffolds after 1 day and 7 days. The proliferation increased to almost 500% for PCL – 3 min MNPs and to more than 600% for PCL – 3 min Si-MNPs after 7 days of incubation with the samples compared to the control (PCL scaffold), further proof of the biocompatibility of nanoparticles scaffolds, as well as a good environment for cell proliferation.

Moreover, the fluorescence images showed the presence of the cells attached to the scaffolds with MNPs and Si-MNPs coating.

In conclusion, the developed scaffolds in PCL with a MNPs or Si-MNPs coating were not cytotoxic, they had slightly antioxidant and antibacterial activity, and they were a good environment for cell proliferation, so they can be good candidates for bone cancer applications.

The samples had also a slightly antioxidant and antibacterial activity, so further studies in these fields could also be considered.

They probably could release nanoparticles in medium, thus, further investigations should be carried out, such as ion release.

These scaffolds could be used for bone regeneration after surgical cancer removal. After surgery, the bone presents defects, and the scaffold, in particular, that one with Si-MNPs coating could stimulate bone regeneration due to bioactive behavior.

As far as future aspects are concerned, one might think to functionalize the scaffolds with other molecules to have a better response in vitro. For example, it could be thought to use growth factors for bone regeneration.

These scaffolds could be used for hyperthermia, due to an external electromagnetic field to allow the heat release by the MNPs up to about 43°C, a temperature that could kill cancer cells. Before their use in the hyperthermia field, it is necessary to carry out studies about scaffolds' behavior at high temperatures, because PCL has a melting temperature point of 60°C, and a glass transition temperature of -60°C, and if this method is used with magnetic particles on the scaffold, PCL could soften. Thus, it should be tested the mechanical behavior of PCL scaffolds with MNPs or Si-MNPs coating at the critical temperature of 43°C, to assess the mechanical tightness of scaffolds during hyperthermic treatment.

Another study that could be carried out on the scaffolds is the evaluation of a hyperthermic effect, to understand whether the scaffolds release heat. In addition, it could also be assessed whether, with an activated magnetic field, cells proliferate more or less than under normal conditions.

References

- [1] Chen, H., & Yao, Y. (2022). Progress of biomaterials for bone tumor therapy. *Journal of Biomaterials Applications*, 36(6), 945–955.
<https://doi.org/10.1177/08853282211035236>
- [2] Ferguson, J. L., & Turner, S. P. (2018). Bone cancer: Diagnosis and treatment principles. *American Family Physician*, 98(4), 205–213.
- [3] COOPER, G. (1951). Bone cancer. *Virginia Medical Monthly*, 78(12), 654.
<https://doi.org/10.6004/jnccn.2013.0088>
- [4] Liao, J., Han, R., Wu, Y., & Qian, Z. (2021). Review of a new bone tumor therapy strategy based on bifunctional biomaterials. *Bone Research*, 9(1).
<https://doi.org/10.1038/s41413-021-00139-z>
- [5] Matteo Bruno Lodi & Alessandro Fanti. Biomedical Applications of Biomaterials Functionalized with Magnetic Nanoparticles
- [6] Spoială, A., Ilie, C. I., Crăciun, L. N., Fikai, D., Fikai, A., & Andronescu, E. (2021). Magnetite-silica core/shell nanostructures: From surface functionalization towards biomedical applications—a review. *Applied Sciences (Switzerland)*, 11(22), 1–21.
<https://doi.org/10.3390/app112211075>
- [7] Tran, N., & Webster, T. J. (2010). Magnetic nanoparticles: Biomedical applications and challenges. *Journal of Materials Chemistry*, 20(40), 8760–8767.
<https://doi.org/10.1039/c0jm00994f>
- [8] Issa, B., Obaidat, I. M., Albiss, B. A., & Haik, Y. (2013). Magnetic nanoparticles: Surface effects and properties related to biomedicine applications. *International Journal of Molecular Sciences*, 14(11), 21266–21305. <https://doi.org/10.3390/ijms141121266>
- [9] Appunti del corso di Bionanotecnologie (2019-2020), PoliTo
- [10] Wu, W., Wu, Z., Yu, T., Jiang, C., & Kim, W. S. (2015). Recent progress on magnetic iron oxide nanoparticles: Synthesis, surface functional strategies and biomedical applications. *Science and Technology of Advanced Materials*, 16(2), 23501.
<https://doi.org/10.1088/1468-6996/16/2/023501>
- [11] Marghussian, V. (2015). Magnetic Properties of Nano-Glass Ceramics. In *Nano-Glass Ceramics*. <https://doi.org/10.1016/b978-0-323-35386-1.00004-9>
- [12] Deatsch, A. E., & Evans, B. A. (2014). Heating efficiency in magnetic nanoparticle hyperthermia. *Journal of Magnetism and Magnetic Materials*, 354, 163–172.
<https://doi.org/10.1016/j.jmmm.2013.11.006>
- [13] Borroni, E., Miola, M., Ferraris, S., Ricci, G., Žužek Rožman, K., Kostevšek, N., Catizone, A., Rimondini, L., Prat, M., Verné, E., & Follenzi, A. (2017). Tumor targeting by lentiviral

- vectors combined with magnetic nanoparticles in mice. *Acta Biomaterialia*, 59, 303–316. <https://doi.org/10.1016/j.actbio.2017.07.007>
- [14] de Mendonça, E. S. D. T., de Faria, A. C. B., Dias, S. C. L., Aragón, F. F. H., Mantilla, J. C., Coaquira, J. A. H., & Dias, J. A. (2019). Effects of silica coating on the magnetic properties of magnetite nanoparticles. In *Surfaces and Interfaces* (Vol. 14). <https://doi.org/10.1016/j.surfin.2018.11.005>
- [15] Kade, J. C., & Dalton, P. D. (2021). Polymers for Melt Electrowriting. *Advanced Healthcare Materials*, 10(1). <https://doi.org/10.1002/adhm.202001232>
- [16] Abdal-hay, A., Abbasi, N., Gwiazda, M., Hamlet, S., & Ivanovski, S. (2018). Novel polycaprolactone/hydroxyapatite nanocomposite fibrous scaffolds by direct melt-electrospinning writing. *European Polymer Journal*, 105(April), 257–264. <https://doi.org/10.1016/j.eurpolymj.2018.05.034>
- [17] Muerza-Cascante, M. L., Shokoohmand, A., Khosrotehrani, K., Haylock, D., Dalton, P. D., Hutmacher, D. W., & Loessner, D. (2017). Endosteal-like extracellular matrix expression on melt electrospun written scaffolds. *Acta Biomaterialia*, 52, 145–158. <https://doi.org/10.1016/j.actbio.2016.12.040>
- [18] Yoshida, M., Turner, P. R., Ali, M. A., & Cabral, J. D. (2021). Three-Dimensional Melt-Electrowritten Polycaprolactone/Chitosan Scaffolds Enhance Mesenchymal Stem Cell Behavior. *ACS Applied Bio Materials*, 4(2), 1319–1329. <https://doi.org/10.1021/acsabm.0c01213>
- [19] Hrynevich, A., Elçi, B., Haigh, J. N., McMaster, R., Youssef, A., Blum, C., Blunk, T., Hochleitner, G., Groll, J., & Dalton, P. D. (2018). Dimension-Based Design of Melt Electrowritten Scaffolds. *Small*, 14(22), 1–6. <https://doi.org/10.1002/sml.201800232>
- [20] Youssef, A., Hrynevich, A., Fladeland, L., Balles, A., Groll, J., Dalton, P. D., & Zabler, S. (2019). The Impact of Melt Electrowritten Scaffold Design on Porosity Determined by X-Ray Microtomography. *Tissue Engineering - Part C: Methods*, 25(6), 367–378. <https://doi.org/10.1089/ten.tec.2018.0373>
- [21] Sonnleitner, D., Schäfer, N., Wieland, A., Fischer, L., Pasberg, P., Thievessen, I., & Lang, G. (2021). PCL micro-dumbbells – A new class of polymeric particles reveals morphological biofunctionality. *Applied Materials Today*, 24, 101097. <https://doi.org/10.1016/j.apmt.2021.101097>
- [22] Brown, T. D., Dalton, P. D., & Hutmacher, D. W. (2011). Direct writing by way of melt electrospinning. *Advanced Materials*, 23(47), 5651–5657. <https://doi.org/10.1002/adma.201103482>
- [23] Miola, M., Bellare, A., Laviano, F., Gerbaldo, R., & Verné, E. (2019). Bioactive superparamagnetic nanoparticles for multifunctional composite bone cements. *Ceramics International*, 45(12), 14533–14545. <https://doi.org/10.1016/j.ceramint.2019.04.170>

- [24] Fan, D., Wang, Q., Zhu, T., Wang, H., Liu, B., Wang, Y., Liu, Z., Liu, X., Fan, D., & Wang, X. (2020). Recent Advances of Magnetic Nanomaterials in Bone Tissue Repair. *Frontiers in Chemistry*, 8(September), 1–15. <https://doi.org/10.3389/fchem.2020.00745>
- [25] Gesim_BIOSCAFFOLDER31_web.pdf
- [26] Zhou, Z. X., Chen, Y. R., Zhang, J. Y., Jiang, D., Yuan, F. Z., Mao, Z. M., Yang, F., Jiang, W. B., Wang, X., & Yu, J. K. (2020). Facile Strategy on Hydrophilic Modification of Poly(ϵ -caprolactone) Scaffolds for Assisting Tissue-Engineered Meniscus Constructs In Vitro. *Frontiers in Pharmacology*, 11(May), 1–11. <https://doi.org/10.3389/fphar.2020.00471>
- [27] Niemczyk-Soczynska, B., Gradys, A., & Sajkiewicz, P. (2020). Hydrophilic surface functionalization of electrospun nanofibrous scaffolds in tissue engineering. *Polymers*, 12(11), 1–20. <https://doi.org/10.3390/polym12112636>
- [28] Muzio, G., Miola, M., Ferraris, S., Maggiora, M., Bertone, E., Puccinelli, M. P., Ricci, M., Borroni, E., Canuto, R. A., Verné, E., & Follenzi, A. (2017). Innovative superparamagnetic iron-oxide nanoparticles coated with silica and conjugated with linoleic acid: Effect on tumor cell growth and viability. *Materials Science and Engineering C*, 76, 439–447. <https://doi.org/10.1016/j.msec.2017.03.063>
- [29] Oltolina, F., Colangelo, D., Miletto, I., Clemente, N., Miola, M., Verné, E., Prat, M., & Follenzi, A. (2019). Tumor targeting by monoclonal antibody functionalized magnetic nanoparticles. *Nanomaterials*, 9(11). <https://doi.org/10.3390/nano9111575>
- [30] Dheyab, M. A., Aziz, A. A., Jameel, M. S., Noqta, O. A., Khaniabadi, P. M., & Mehrdel, B. (2020). Simple rapid stabilization method through citric acid modification for magnetite nanoparticles. *Scientific Reports*, 10(1), 1–8. <https://doi.org/10.1038/s41598-020-67869-8>
- [31] Campelj, S., Makovec, D., & Drogenik, M. (2008). Preparation and properties of water-based magnetic fluids. *Journal of Physics Condensed Matter*, 20(20). <https://doi.org/10.1088/0953-8984/20/20/204101>
- [32] Deng, Y. H., Wang, C. C., Hu, J. H., Yang, W. L., & Fu, S. K. (2005). Investigation of formation of silica-coated magnetite nanoparticles via sol-gel approach. *Colloids and Surfaces A: Physicochemical and Engineering Aspects*, 262(1–3), 87–93. <https://doi.org/10.1016/j.colsurfa.2005.04.009>
- [33] Unalan, I., Endlein, S. J., Slavik, B., Buettner, A., Goldmann, W. H., Detsch, R., & Boccaccini, A. R. (n.d.). □□□□□ 2.Pdf. Clv.
- [34] Bouafia, A., Laouini, S. E., Khelef, A., Tedjani, M. L., & Guemari, F. (2021). Effect of Ferric Chloride Concentration on the Type of Magnetite (Fe₃O₄) Nanoparticles Biosynthesized by Aqueous Leaves Extract of Artemisia and Assessment of Their Antioxidant Activities. *Journal of Cluster Science*, 32(4), 1033–1041. <https://doi.org/10.1007/s10876-020-01868-7>
- [35] Kim, J. J., Singh, R. K., Seo, S. J., Kim, T. H., Kim, J. H., Lee, E. J., & Kim, H. W. (2014). Magnetic scaffolds of polycaprolactone with functionalized magnetite nanoparticles:

Physicochemical, mechanical, and biological properties effective for bone regeneration. *RSC Advances*, 4(33), 17325–17336. <https://doi.org/10.1039/c4ra00040d>

- [36] Lin, T. S., & Jeng, S. F. (2006). Full-thickness skin graft as a one-stage debulking procedure after free flap reconstruction for the lower leg. *Plastic and Reconstructive Surgery*, 118(2), 408–412. <https://doi.org/10.1097/01.prs.0000227624.99710.ee>
- [37] <https://www.cancer.gov/about-cancer/causes-prevention/risk/infectious-agents>
- [38] Elsland, D., & Neefjes, J. (2018). Bacterial infections and cancer. *EMBO Reports*, 19(11), 1–11. <https://doi.org/10.15252/embr.201846632>
- [39] Allafchian, A., & Hosseini, S. S. (2019). Antibacterial magnetic nanoparticles for therapeutics: A review. *IET Nanobiotechnology*, 13(8), 786–799. <https://doi.org/10.1049/iet-nbt.2019.0146>
- [40] Chaurasia, A. K., Thorat, N. D., Tandon, A., Kim, J. H., Park, S. H., & Kim, K. K. (2016). Coupling of radiofrequency with magnetic nanoparticles treatment as an alternative physical antibacterial strategy against multiple drug resistant bacteria. *Scientific Reports*, 6(August), 1–13. <https://doi.org/10.1038/srep33662>
- [41] Taimoory, S. M., Rahdar, A., Aliahmad, M., Sadeghfar, F., Hajinezhad, M. R., Jahantigh, M., Shahbazi, P., & Trant, J. F. (2018). The synthesis and characterization of a magnetite nanoparticle with potent antibacterial activity and low mammalian toxicity. *Journal of Molecular Liquids*, 265(2017), 96–104. <https://doi.org/10.1016/j.molliq.2018.05.105>
- [42] Prabhu, Y. T., Rao, K. V., Kumari, B. S., Kumar, V. S. S., & Pavani, T. (2015). Synthesis of Fe₃O₄ nanoparticles and its antibacterial application. *International Nano Letters*, 5(2), 85–92. <https://doi.org/10.1007/s40089-015-0141-z>
- [43] Unalan, I., Fuggerer, T., Slavik, B., Buettner, A., & Boccaccini, A. R. (2021). Antibacterial and antioxidant activity of cinnamon essential oil-laden 45S5 bioactive glass/soy protein composite scaffolds for the treatment of bone infections and oxidative stress. *Materials Science and Engineering C*, 128(July), 112320. <https://doi.org/10.1016/j.msec.2021.112320>
- [44] Abbasi, N., Abdal-Hay, A., Hamlet, S., Graham, E., Ivanovski, S., Tourlomousis, F., Jia, C., Karydis, T., Mershin, A., Wang, H., Kalyon, D. M., & Chang, R. C. (2019). Effects of Gradient and Offset Architectures on the Mechanical and Biological Properties of 3-D Melt Electrowritten (MEW) Scaffolds. *Microsystems and Nanoengineering*, 5(1), 3448–3461. <https://doi.org/10.1021/acsbiomaterials.8b01456>
- [45] Mueller, K. M. A., Topping, G. J., Schwaminger, S. P., Zou, Y., Rojas-González, D. M., De-Juan-Pardo, E. M., Berensmeier, S., Schilling, F., & Mela, P. (2021). Visualization of USPIO-labeled melt-electrowritten scaffolds by non-invasive magnetic resonance imaging. *Biomaterials Science*, 9(13), 4607–4612. <https://doi.org/10.1039/d1bm00461a>

- [46] Turlomousis, F., Jia, C., Karydis, T., Mershin, A., Wang, H., Kalyon, D. M., & Chang, R. C. (2019). Machine learning metrology of cell confinement in melt electrowritten three-dimensional biomaterial substrates. *Microsystems and Nanoengineering*, 5(1). <https://doi.org/10.1038/s41378-019-0055-4>
- [47] Blaudez, F., Ivanovski, S., Ipe, D., & Vaquette, C. (2020). A comprehensive comparison of cell seeding methods using highly porous melt electrowriting scaffolds. *Materials Science and Engineering C*, 117(June), 111282. <https://doi.org/10.1016/j.msec.2020.111282>
- [48] Hochleitner, G., Fürsattel, E., Giesa, R., Groll, J., Schmidt, H. W., & Dalton, P. D. (2018). Melt Electrowriting of Thermoplastic Elastomers. *Macromolecular Rapid Communications*, 39(10), 1–7. <https://doi.org/10.1002/marc.201800055>
- [49] Kim, J., Bakirci, E., O'Neill, K. L., Hrynevich, A., & Dalton, P. D. (2021). Fiber Bridging during Melt Electrowriting of Poly(ϵ -Caprolactone) and the Influence of Fiber Diameter and Wall Height. *Macromolecular Materials and Engineering*, 306(3). <https://doi.org/10.1002/mame.202000685>
- [50] Ali, S., Khatri, Z., Oh, K. W., Kim, I. S., & Kim, S. H. (2014). Preparation and characterization of hybrid polycaprolactone/cellulose ultrafine fibers via electrospinning. *Macromolecular Research*, 22(5), 562–568. <https://doi.org/10.1007/s13233-014-2078-x>
- [51] Pérez-Álvarez, L., Ruiz-Rubio, L., Moreno, I., & Vilas-Vilela, J. L. (2019). Characterization and optimization of the alkaline hydrolysis of polyacrylonitrile membranes. *Polymers*, 11(11), 1–11. <https://doi.org/10.3390/polym11111843>
- [52] Hui, B. H., & Salimi, M. N. (2020). Production of Iron Oxide Nanoparticles by Co-Precipitation method with Optimization Studies of Processing Temperature, pH and Stirring Rate. *IOP Conference Series: Materials Science and Engineering*, 743(1). <https://doi.org/10.1088/1757-899X/743/1/012036>
- [53] Padalia, D., Johri, U. C., & Zaidi, M. G. H. (2012). Study of cerium doped magnetite (Fe₃O₄:Ce)/PMMA nanocomposites. *Physica B: Condensed Matter*, 407(5), 838–843. <https://doi.org/10.1016/j.physb.2011.12.016>
- [54] Izza Taib, N., G. St. Pierre, T., C. Woodward, R., & J. House, M. (2019). Magnetic Properties of Magnetite Nanoparticles (Fe₃O₄-NPs) Coated with Mesoporous Silica by Surfactant Templated Sol-Gel Method. *International Journal of Engineering & Technology*, 7(4.14), 533. <https://doi.org/10.14419/ijet.v7i4.14.27785>
- [55] Mohamed, N., Hessen, O. E. A., & Mohammed, H. S. (2021). Thermal stability, paramagnetic properties, morphology and antioxidant activity of iron oxide nanoparticles synthesized by chemical and green methods. *Inorganic Chemistry Communications*, 128(March), 108572. <https://doi.org/10.1016/j.inoche.2021.108572>
- [56] Vitta, Y., Figueroa, M., Calderon, M., & Ciangherotti, C. (2020). Synthesis of iron nanoparticles from aqueous extract of *Eucalyptus robusta* Sm and evaluation of antioxidant and antimicrobial activity. *Materials Science for Energy Technologies*, 3, 97–103. <https://doi.org/10.1016/j.mset.2019.10.014>

- [57] Shuai, C., Yang, W., He, C., Peng, S., Gao, C., Yang, Y., Qi, F., & Feng, P. (2020). A magnetic micro-environment in scaffolds for stimulating bone regeneration. *Materials and Design*, 185, 108275. <https://doi.org/10.1016/j.matdes.2019.108275>
- [58] Maleki-Ghaleh, H., Aghaie, E., Nadernezhad, A., Zargarzadeh, M., Khakzad, A., Shakeri, M. S., Beygi Khosrowshahi, Y., & Siadati, M. H. (2016). Influence of Fe₃O₄ Nanoparticles in Hydroxyapatite Scaffolds on Proliferation of Primary Human Fibroblast Cells. *Journal of Materials Engineering and Performance*, 25(6), 2331–2339. <https://doi.org/10.1007/s11665-016-2086-4>
- [59] Kim, J. J., Singh, R. K., Seo, S. J., Kim, T. H., Kim, J. H., Lee, E. J., & Kim, H. W. (2014). Magnetic scaffolds of polycaprolactone with functionalized magnetite nanoparticles: Physicochemical, mechanical, and biological properties effective for bone regeneration. *RSC Advances*, 4(33), 17325–17336. <https://doi.org/10.1039/c4ra00040d>
- [60] Rezaei, V., Mirzaei, E., Taghizadeh, S. M., Berenjian, A., & Ebrahiminezhad, A. (2021). Nano iron oxide-PCL composite as an improved soft tissue scaffold. *Processes*, 9(9). <https://doi.org/10.3390/pr9091559>
- [61] Rahman, M. M., Islam, M. B., Biswas, M., & Khurshid Alam, A. H. M. (2015). In vitro antioxidant and free radical scavenging activity of different parts of *Tabebuia pallida* growing in Bangladesh. *BMC Research Notes*, 8(1), 1–9. <https://doi.org/10.1186/s13104-015-1618-6>
- [62] National Cancer Institute <https://www.cancer.gov/about-cancer/causes-prevention/risk/diet/antioxidants-fact-sheet#what-are-antioxidants>
- [63] Wu, X., Dai, H., Xu, C., Liu, L., & Li, S. (2019). Citric acid modification of a polymer exhibits antioxidant and anti-inflammatory properties in stem cells and tissues. *Journal of Biomedical Materials Research - Part A*, 107(11), 2414–2424. <https://doi.org/10.1002/jbm.a.36748>
- [64] Abdel-Salam, O. M. E., Youness, E. R., Mohammed, N. A., Morsy, S. M. Y., Omara, E. A., & Sleem, A. A. (2014). Citric acid effects on brain and liver oxidative stress in lipopolysaccharide-treated mice. *Journal of Medicinal Food*, 17(5), 588–598. <https://doi.org/10.1089/jmf.2013.0065>
- [65] Robinson, W. S., & Lutwick, L. I. (1976). The Virus of Hepatitis, Type B. *New England Journal of Medicine*, 295(21), 1168–1175. <https://doi.org/10.1056/nejm197611182952105>